Cell Stem Cell

Resource

3D ECM-rich environment sustains the identity of naive human iPSCs

Graphical abstract

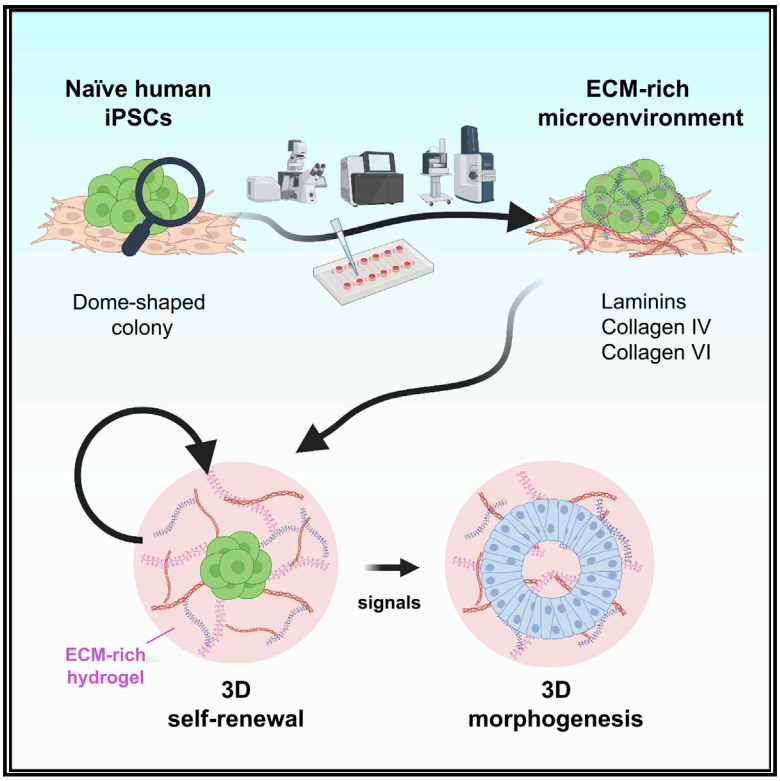

Authors

Elisa Cesare, Anna Urciuolo, Hannah T. Stuart, ..., Davide Cacchiarelli, Camilla Luni, Nicola Elvassore

Correspondence

n.elvassore@ucl.ac.uk

In brief

The extracellular matrix (ECM) microenvironment is emerging as a player in early human development. Cesare et al. demonstrate that naive hiPSCs exhibit a self-organized ECM-rich microenvironment *in vitro*, which sustains their identity. They developed a 3D ECM-rich feeder-free culture system that supports naive hiPSC self-renewal or timely developmental morphogenesis.

Highlights

- ECM proteins are secreted and deposited around naive hiPSC dome-shaped colonies
- Laminins are produced by naive hiPSCs and support their clonogenicity
- 3D ECM-rich environment preserves long-term feeder-free naive hiPSC self-renewal
- 3D-cultured naive hiPSCs undergo developmental morphogenesis in response to signal cues

Cesare et al., 2022, Cell Stem Cell *29*, 1703–1717
December 1, 2022
https://doi.org/10.1016/j.stem.2022.11.011

CellPress

Cell Stem Cell

CellPress

Resource

3D ECM-rich environment sustains the identity of naive human iPSCs

Elisa Cesare,[1,2,19] Anna Urciuolo,[3,4,5,19] Hannah T. Stuart,[1,2,6,7,19] Erika Torchio,[2] Alessia Gesualdo,[1] Cecilia Laterza,[1,2] Onelia Gagliano,[1,2] Sebastian Martewicz,[8] Meihua Cui,[8] Anna Manfredi,[9,10] Lucio Di Filippo,[9,10] Patrizia Sabatelli,[11,12] Stefano Squarzoni,[11,12] Irene Zorzan,[13] Riccardo M. Betto,[5] Graziano Martello,[14] Davide Cacchiarelli,[9,15,16] Camilla Luni,[8,17] and Nicola Elvassore[1,2,3,18,*]

[1]Department of Industrial Engineering, University of Padova, 6/a Via Gradenigo, Padova 35131, Italy
[2]Veneto Institute of Molecular Medicine, 2 Via Orus, Padova 35131, Italy
[3]University College London Great Ormond Street Institute of Child Health, 30 Guilford Street, London WC1N 1EH, UK
[4]Institute of Pediatric Research IRP, Corso Stati Uniti, Padova 35127, Italy
[5]Department of Molecular Medicine, University of Padova, Via G. Colombo 3, 35131 Padova, Italy
[6]The Francis Crick Institute, 1 Midland Road, London NW1 1AT, UK
[7]Research Institute of Molecular Pathology (IMP), Vienna BioCenter (VBC), Campus-Vienna-BioCenter 1, 1030 Vienna, Austria
[8]Shanghai Institute for Advanced Immunochemical Studies (SIAIS), ShanghaiTech University, 393 Middle Huaxia Road, Pudong, Shanghai 201210, China
[9]Telethon Institute of Genetics and Medicine (TIGEM), Armenise/Harvard Laboratory of Integrative Genomics, Pozzuoli, Italy
[10]Next Generation Diagnostic srl, Pozzuoli, Italy
[11]CNR - Institute of Molecular Genetics "Luigi Luca Cavalli-Sforza" - Unit of Bologna, Bologna, Italy
[12]IRCCS-Istituto Ortopedico Rizzoli, Bologna, Italy
[13]Epigenetics Programme, Babraham Institute, CB22 3AT Cambridge, UK
[14]Department of Biology, University of Padova, Via G. Colombo 3, Padova 35131, Italy
[15]Department of Translational Medicine, University of Naples "Federico II", Naples, Italy
[16]School for Advanced Studies, Genomics and Experimental Medicine Program, University of Naples "Federico II", Naples, Italy
[17]Department of Civil, Chemical, Environmental, and Materials Engineering (DICAM), University of Bologna, Via Terracini 28, Bologna 40131, Italy
[18]Lead contact
[19]These authors contributed equally
*Correspondence: n.elvassore@ucl.ac.uk
https://doi.org/10.1016/j.stem.2022.11.011

SUMMARY

The establishment of *in vitro* naive human pluripotent stem cell cultures opened new perspectives for the study of early events in human development. The role of several transcription factors and signaling pathways have been characterized during maintenance of human naive pluripotency. However, little is known about the role exerted by the extracellular matrix (ECM) and its three-dimensional (3D) organization. Here, using an unbiased and integrated approach combining microfluidic cultures with transcriptional, proteomic, and secretome analyses, we found that naive, but not primed, hiPSC colonies are characterized by a self-organized ECM-rich microenvironment. Based on this, we developed a 3D culture system that supports robust long-term feeder-free self-renewal of naive hiPSCs and also allows direct and timely developmental morphogenesis simply by modulating the signaling environment. Our study opens new perspectives for future applications of naive hiPSCs to study critical stages of human development in 3D starting from a single cell.

INTRODUCTION

Human pluripotent stem cells (hPSCs), including human embryonic stem cells (hESCs) and human induced pluripotent stem cells (hiPSCs), can self-renew indefinitely in culture while maintaining the ability to give rise to all lineages of the human body.[1] When cultured *in vitro*, hPSCs can be captured within two distinct pluripotent stages,[2] named naive and primed, which *in vivo* correspond to the pre-implantation and the post-implantation pluripotent epiblast cells, respectively.[3,4] Compared to primed hPSCs, and in light of their earlier developmental identity, naive hPSCs are of great interest since they open new opportunities to study pre- and peri-implantation human development,[5,6] as well as offering an epigenetic *tabula rasa*.[7–9]

Naive hPSCs *in vitro* show an intrinsic tendency to organize into compact dome-shaped three-dimensional (3D) colonies,[2,3] mimicking the spatial organization of the pre-implantation epiblast *in vivo*.[10] In the naive epiblast, the three-dimensionality is provided by the surrounding primitive endoderm and trophectoderm, which contribute to embryonic development by

secreting morphogens, but also through the deposition and remodeling of the extracellular matrix (ECM).[11,12]

Efforts have been made to understand the network of signaling cues *in vivo* to inform the induction, stabilization, and maintenance of naive hPSCs *in vitro.*[13] Based on knowledge derived from mouse naive PSC cultures[14,15] and transcriptomic analyses of pre-implantation human and primate embryos,[4,7,16] various culture conditions have been optimized by testing soluble signals associated with the naive pluripotent gene regulatory network. These culture regimes allowed the *in vitro* capture of naive hPSC states in two-dimensional (2D) culture platforms.[2,5,13,17–20]

Concerning the ECM, however, little is known about the deposition and remodeling of its components in the 3D environment of naive hPSCs. In early mammalian development, an endogenous basement membrane lines the boundary of the epiblast and primitive endoderm and has been shown to have a role in guiding epiblast and embryo early morphogenesis.[11] Thus, ECM components are likely to contribute to shaping the dynamic environment that influences and guides cell morphology, survival, proliferation, and differentiation. Naive hPSCs *in vitro* are routinely cultured on a feeder layer of mitotically inactivated murine embryonic fibroblasts (MEFs) for long-term maintenance of their phenotype. It has been shown that MEFs produce and secrete ECM proteins and ECM remodeling enzymes in human primed PSC cultures.[21] This supports the hypothesis that MEFs might contribute to the maintenance of naive 3D dome-shaped morphology and thus naive phenotype by secreting and remodeling ECM proteins.

Since the use of MEFs has many limitations for the application of naive hPSCs both in basic research and with clinical outlook, it is important to replace MEFs and develop feeder-free culture regimes. For primed hPSC *in vitro* cultures, the use of single ECM proteins as culture coating has been successfully established.[22,23] On the contrary, few naive hPSC feeder-free culture conditions have been published, which rely on coating with gel mixtures, high concentrations of ECM proteins such as laminins, or addition of gel mixtures to the media.[18,24]

We reasoned that by first characterizing the ECM microenvironment of naive hiPSCs, we will better understand how to rationally support them in their naive state *in vitro* and better recapitulate the 3D environment experienced by the pre-implantation epiblast *in vivo*.

Here, we take an unbiased integrative approach including microfluidic cell cultures, proteomic analyses of secretome and lysate, transcriptomics, electron microscopy, and immunofluorescence to characterize the ECM expressed and deposited around naive hiPSC colonies. Then, we apply this knowledge to create a robust, feeder-free 3D culture system based on ECM-rich hydrogels that can sustain naive identity long-term or permit timely 3D developmental morphogenesis in response to signaling cues.

RESULTS

Naive hiPSC colonies are surrounded by a 3D ECM-rich microenvironment

To ascertain whether morphological features are correlated with the pluripotency state of hiPSCs, we evaluated colony architecture, cell morphology, and ECM deposition by electron microscopy. Scanning electron microscopy (SEM) revealed a flat epithelial morphology of primed colonies, in which single cells and their boundaries are clearly visible with no distinguishable ECM deposition (Figure 1A). Conversely, naive compact dome-shaped 3D colonies presented a layer of ECM on their surface, precluding visualization of individual cells within a colony (Figure 1A). To confirm these findings, colonies were embedded in resin, and ultrathin sections were analyzed by transmission electron microscopy (TEM). In agreement with SEM results, we observed a filamentous network, consistent with ECM protein deposition, present at the external surface of naive colonies but absent from primed hiPSCs (Figure 1B, black stars). For both primed and naive colonies, ECM deposition was not evident in the intercellular space (Figure 1B, black arrows). In sum, these data indicated that, unlike primed hiPSCs, naive hiPSCs organize into dome-shaped 3D colonies surrounded by an ECM-rich microenvironment.

To better characterize the composition of this ECM microenvironment, we applied an integrative approach that allowed us to investigate transcriptomic, proteomic, and secretome profiles of naive hiPSCs. Microfluidic culture platforms were used to reach high sensitivity for capturing differential secreted proteins together with transcriptomic analyses. Indeed, microfluidic culture systems are known to enhance the accumulation of cell-secreted signals and soluble factors within the confined volume of the device, thus better mimicking autocrine and paracrine signals that exist in the interstitial spaces *in vivo* and resulting in enhanced ECM deposition and remodeling.[25–28]

To allow comparison unconfounded by parental line variability, we derived isogenic primed hiPSCs from HPD06 naive hiPSCs (Figure S1A). Appropriate naive or primed identities of isogenic hiPSCs were confirmed by immunofluorescence for specific markers: KLF17 (naive), TFE3 (naive), SSEA4 (primed), and OCT4 (shared) (Figure S1A). We confirmed that naive and primed hiPSCs maintain their respective identities when cultured in microfluidic platforms by bulk RNA-sequencing and immunofluorescence (Figures 1C, 1D, S1B, and S1C; Table S1). Together with cell identity maintenance, microfluidic devices also preserved cell morphology and ECM deposition (Figure S1D).

Transcriptome comparison between isogenic naive hiPSCs, primed hiPSCs, or parental fibroblasts showed that each cell type has a distinctive expression of ECM genes (Figure S1E). Cell-type-specific ECM expression profiles were also observed by hierarchical clustering analysis of published RNA-seq datasets (Figure S1F). However, transcription of ECM-coding genes does not guarantee ECM protein production, secretion, and deposition in the extracellular space. Since we also observed differences by electron microscopy analysis, we performed immunostaining on naive and primed hiPSCs to evaluate protein production and deposition of specific ECM components known to be abundant in tissues, such as basement lamina constituents (laminins and collagen type IV)[29] and other components belonging to the reticular lamina (collagen type I and type VI).[29,30] Interestingly, strong deposition and 3D organization of the investigated ECM proteins were observed only around naive colonies, but not primed (Figures 1E and 1F). In particular, collagen type IV and laminins were deposited on the surface of

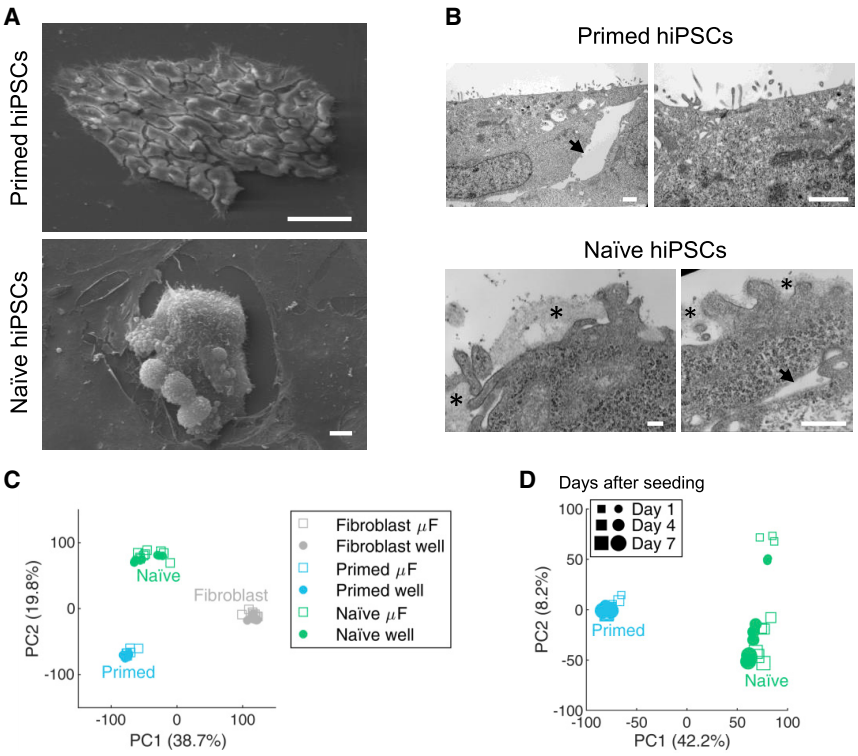

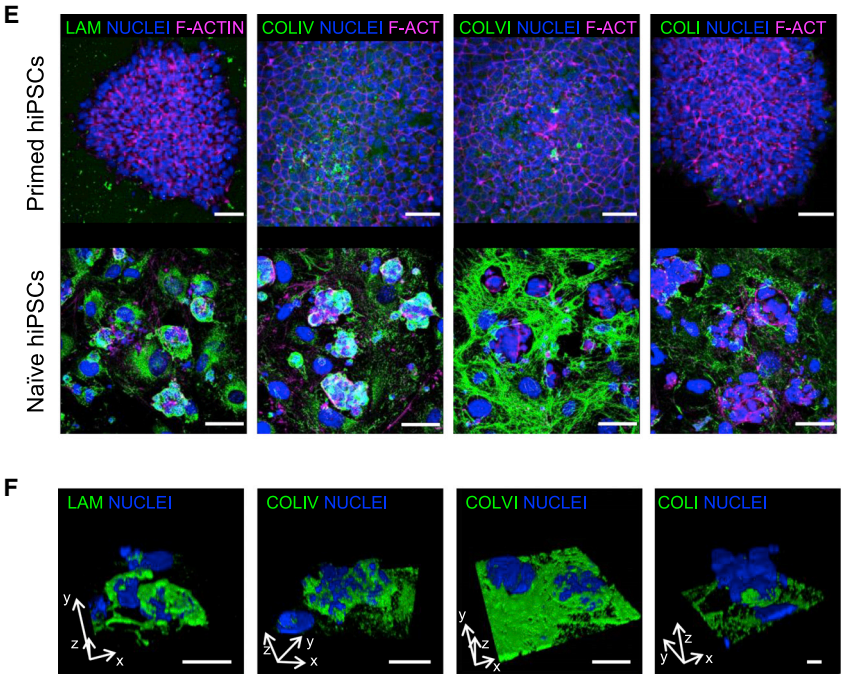

Figure 1. Characterization of naive and primed hiPSCs cultured in microfluidic or conventional devices

(A) Representative scanning electron microscopy (SEM) images showing primed (upper panel) or naive (lower panel) hiPSC colonies. Scale bars, 100 μm.

(B) Representative transmission electron microscopy (TEM) images showing primed (upper panel) or naive (lower panel) hiPSCs. The asterisks indicate ECM deposited at the external surface of cell aggregates. Arrows indicate intercellular spaces. Scale bars, 1 μm.

(C) Principal component analysis (PCA) of isogenic primed (cyan) and naive hiPSCs (green) and fibroblasts (gray) cultured in conventional (well) or microfluidic (μF) devices.

(D) PCA of samples shown in (C), except for fibroblasts, highlighting differences between time points after 1, 4, or 7 days from seeding.

(E) Representative z stack confocal images of isogenic primed (upper panel) or naive (lower panel) hiPSCs immunostained for laminins (LAM, green), collagen type IV (COLIV, green), collagen type VI (COLVI, green), or collagen type I (COLI, green) and F-actin (magenta). Nuclei were stained with Hoechst (blue). Scale bars, 50 μm (upper panels) or 100 μm (lower panels).

(F) Representative 3D reconstruction of naive hiPSC cultures immunostained for laminins (LAM, green), collagen type IV (COLIV, green), collagen type VI (COLVI, green), or collagen type I (COLI, green). Nuclei were stained with Hoechst (blue). Scale bars, 25 μm.

naive colonies. In contrast, collagen type VI and collagen type I were organized in microfilaments and mostly deposited around and between colonies, with collagen type I showing a reduced network deposition compared to collagen type VI (Figures 1E and 1F). In accordance with SEM and TEM analysis, all the analyzed ECM proteins were scarcely detected on isogenic primed hiPSCs, and when secreted, they were organized in isolated spots (Figure 1E, upper panels).

Taken together, these data demonstrate that naive and primed pluripotent states are characterized by different expression, production, and deposition of ECM components. Surprisingly, only naive hiPSC colonies exhibited a 3D ECM-rich microenvironment. However, whether this is formed solely by production and deposition of ECM proteins by the naive cells themselves is still unclear due to the presence of MEF feeders in their culture.

Transcriptomic and proteomic analyses reveal that naive cells have a specific ECM fingerprint

To ascertain whether naive cells are themselves able to produce the observed ECM proteins, we transiently cultured naive hiPSCs without MEF feeders in microfluidic devices coated with recombinant Vitronectin (VTN) to clearly distinguish endogenously produced ECM from exogenous single-protein coating. After setting up optimal culture conditions (Figures S2A–S2C), we confirmed ECM production and deposition by immunofluorescent analysis in feeder-free naive hiPSC cultures (Figure 2A). The investigated ECM proteins were detectable from the first days of culture, although less extracellular

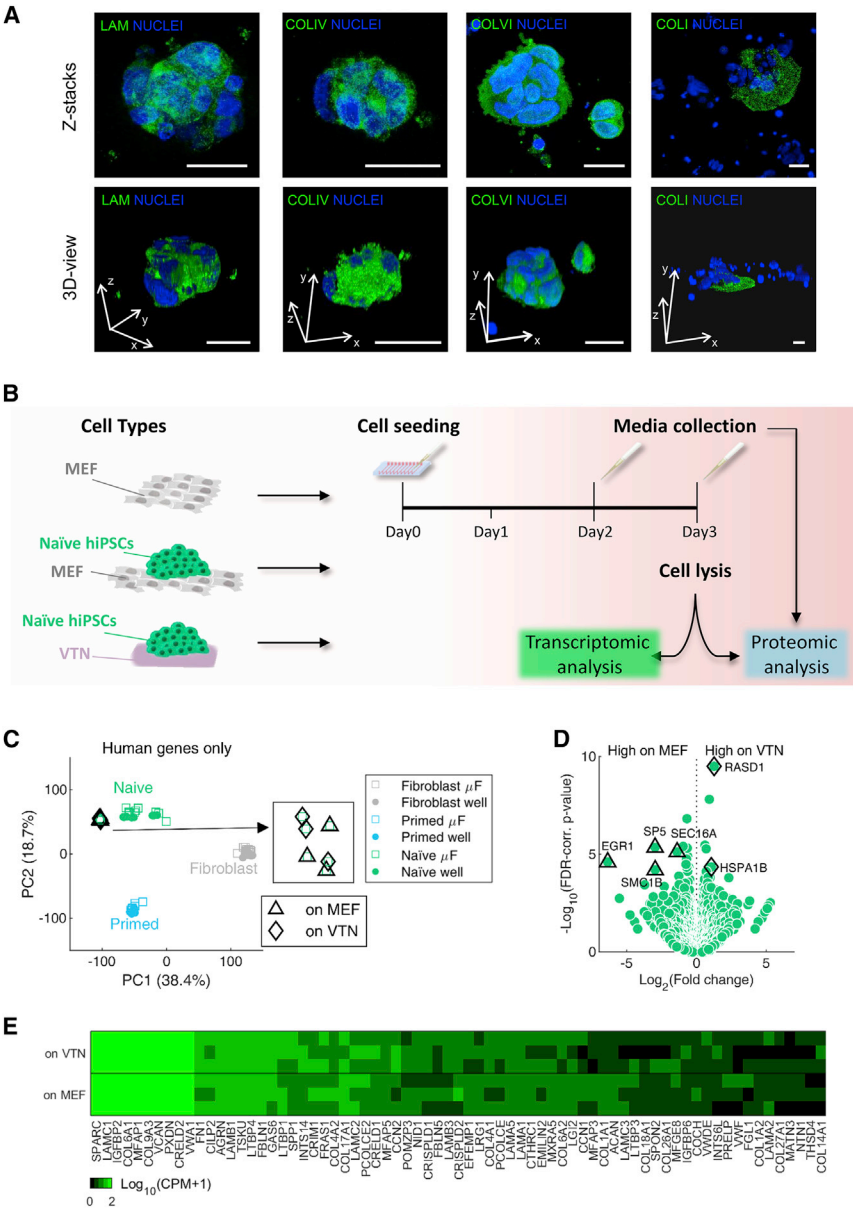

Figure 2. Characterization of a naive hiPSC feeder-free culture and ECM transcriptomic analysis

(A) Representative z stack (upper panels) and 3D reconstruction (lower panels) of naive hiPSC cultures without MEF in microfluidics and immunostained for laminins (LAM, green), collagen type IV (COLIV, green), collagen type VI (COLVI, green), or collagen type I (COLI, green). Nuclei were stained with Hoechst (blue). Scale bars, 25 μm.

(B) Experimental design included three culture conditions in microfluidics: MEF cultured alone on VTN, naive hiPSCs cultured on an MEF feeder layer (mixed cell population), and naive hiPSCs cultured alone on VTN (feeder-free culture). Total RNA and protein lysate were collected at day 3 for RNA-seq analysis and proteomic analysis, respectively. Conditioned media were also collected 2 and 3 days after seeding for proteomic analysis.

(C) PCA of samples shown in Figure 1C, also including naive samples cultured either on MEF or on VTN in microfluidics under hypoxic conditions. Only human genes were included to exclude MEF contribution in the co-culture condition. Inset on the right is an enlargement of the samples indicated to appreciate small spatial variations.

(D) Volcano plot of naive pluripotent stem cell samples cultured with or without feeder layer. DEGs are indicated by black edges (uncorrected p value < 0.05 and absolute fold change >2).

(E) Expression of the most highly expressed core ECM human genes in naive cells cultured on MEF or feeder-free.

deposition was observed in this culture regime compared to naive hiPSCs on MEFs (Figures 2A, S2D, and S2E).

We performed transcriptomic and proteomic analyses comparing 3 different cultures: MEF only, naive hiPSCs on MEF, and naive hiPSCs on VTN. Transcriptional profiling and cell lysate proteomic analyses were conducted 3 days after cell seeding, and conditioned media for secreted protein analysis was collected throughout the culture time (Figure 2B).

Since we aimed to compare the transcriptomic profiles of naive hiPSCs cultured in the presence or absence of MEFs, we confirmed that we could distinguish between human and murine transcripts (Figures S2F and S2G) to focus the subsequent analysis only on human gene expression. PCA analysis (Figure 2C) as well as Volcano plot (Figure 2D) demonstrated strong transcriptional similarity between naive hiPSCs cultured in the presence or absence of MEFs. Interestingly, naive cells expressed several ECM-related genes, including collagens and laminins (Figure 2E). These ECM genes were not significantly differentially expressed between the two culture conditions. Thus, we confirmed that naive hiPSCs express ECM genes independently of the presence or absence of co-cultured MEFs.

Proteomic analyses were performed by tandem mass spectrometry using isobaric tag labeling of an equal amount of protein for each sample to permit a relative quantification of protein production among MEF-only, hiPSCs on MEF, and hiPSCs on VTN samples (Figures S3A–S3D). We identified 2,216 proteins in the cell lysates (Table S2). The majority of differentially abundant proteins (DAPs) were upregulated in naive-containing samples compared to MEF-only culture (Figures 3A and S3E). Enrichment analysis within both Reactome and Gene Ontology - Biological Processes (GO-BP) databases highlighted that cell cycle and protein translation were upregulated in naive hiPSC cultures when compared to MEF-only cultures, consistent with the active proliferation state of naive cells compared to mitotically inactivated MEFs (Figure 3A; Table S2). Independently of the presence or absence of MEFs, naive hiPSCs cultured in microfluidics exhibit a similar proteomic signature (Figure 3B) and, importantly, produce proteins known to build the core ECM (Figures 3C and S3F).[31]

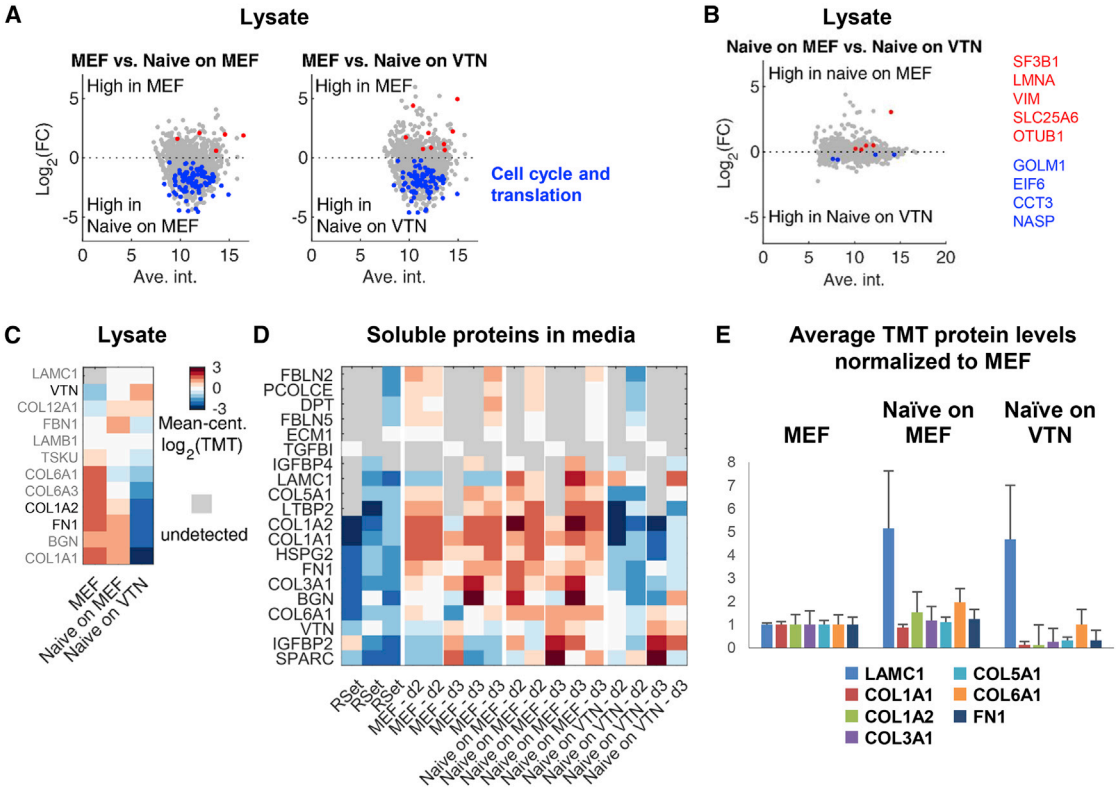

Figure 3. Proteomic analysis highlights the different contributions to ECM environment by MEF and naive pluripotent stem cells

(A and B) Proteomic analysis of lysate samples.

(A) The log2-fold change (log2[FC]) of protein expression in MEF versus naive on MEF (left) and MEF versus naive on VTN (right) is shown as a function of average expression in log-scale in the samples compared. Differentially abundant proteins are marked with higher expression in MEF (red) or in naive samples (blue). Adjacent text shows Gene Ontology enrichment main categories of differentially abundant proteins. Differentially abundant proteins were identified by ANOVA uncorrected p value < 0.05 and Tukey's post-hoc test with p value < 0.05 (n = 3).

(B) The log2(FC) of protein expression in naive on MEF versus naive on VTN samples is shown as a function of average expression in log-scale in the samples compared. Differentially abundant proteins with higher expression in naive on MEF (red) or in naive on VTN samples (blue) are labeled and were identified by ANOVA uncorrected p value < 0.05 and Tukey's post-hoc test with p value < 0.05 (n = 3).

(C) Heatmap showing the relative expression of core ECM proteins in MEF, naive on MEF, and naive on VTN samples (n = 3). Each protein expression was mean centered individually according to the color bar. Proteins detected in sample number n < 3 have their names written in gray. Undetected proteins are colored gray on the heatmap.

(D) Proteomic analysis of soluble proteins accumulated in media. Heatmap showing core ECM proteins detected in RSeT medium, MEF, naive on MEF, or naive on VTN conditioned media after 2 and 3 days of culture. Heatmap color scale is the same as in (C).

(E) Proteomic analysis of soluble proteins accumulated in media collected after 2 and 3 days in culture. Average Tandem Mass Tag (TMT) levels of proteins previously investigated in this work. Data are shown as mean ± SD; n = 4 or 5.

Then, we analyzed the soluble fraction of proteins present within the media collected from the different cell cultures (Table S3). We identified 443 proteins that are accumulated in the media of cells cultured in RSeT™. By differential analysis, we could distinguish cell-secreted proteins from those present in RSeT media such as albumin, transferrin, and insulin (Table S3). In accordance with our previous results (Figures 1E, 1F, and 2A), we confirmed the presence of secreted ECM proteins in naive hiPSC cultures independently of the presence or absence of MEFs (Figure 3D). In particular, the quantification of the level of secreted ECM proteins showed that laminins are enriched in the media of naive hiPSC cultures (Figure 3E). In agreement with transcriptomic analyses, these data demonstrated that naive cells produce and secrete ECM components, especially laminins, even in the absence of feeders. It is important to mention that MEFs, which also produce ECM components (Figures 3A–3C), contribute to the deposition and organization of ECM when co-cultured with naive hiPSCs, with basement membrane component laminins organized in a shell over the 3D naive colony surface (Figure 1E).

Based on these data, we hypothesized that the ECM could have a functional role in the maintenance of the hiPSC naive state. To test this hypothesis, we disrupted the interaction between naive hiPSCs and the ECM during cell culture with small molecules or antibodies directed against specific integrins or ECM proteins (Figure 4A). The performed treatments included a blocking antibody for integrin β1,[32] the non-arginyl-glycyl-aspartic acid (RGD)-based antagonist ATN-161[33–35] to inhibit α5β1 integrins, and polyclonal antibodies that bind ECM proteins, laminins, collagen IV, and collagen VI that we found to

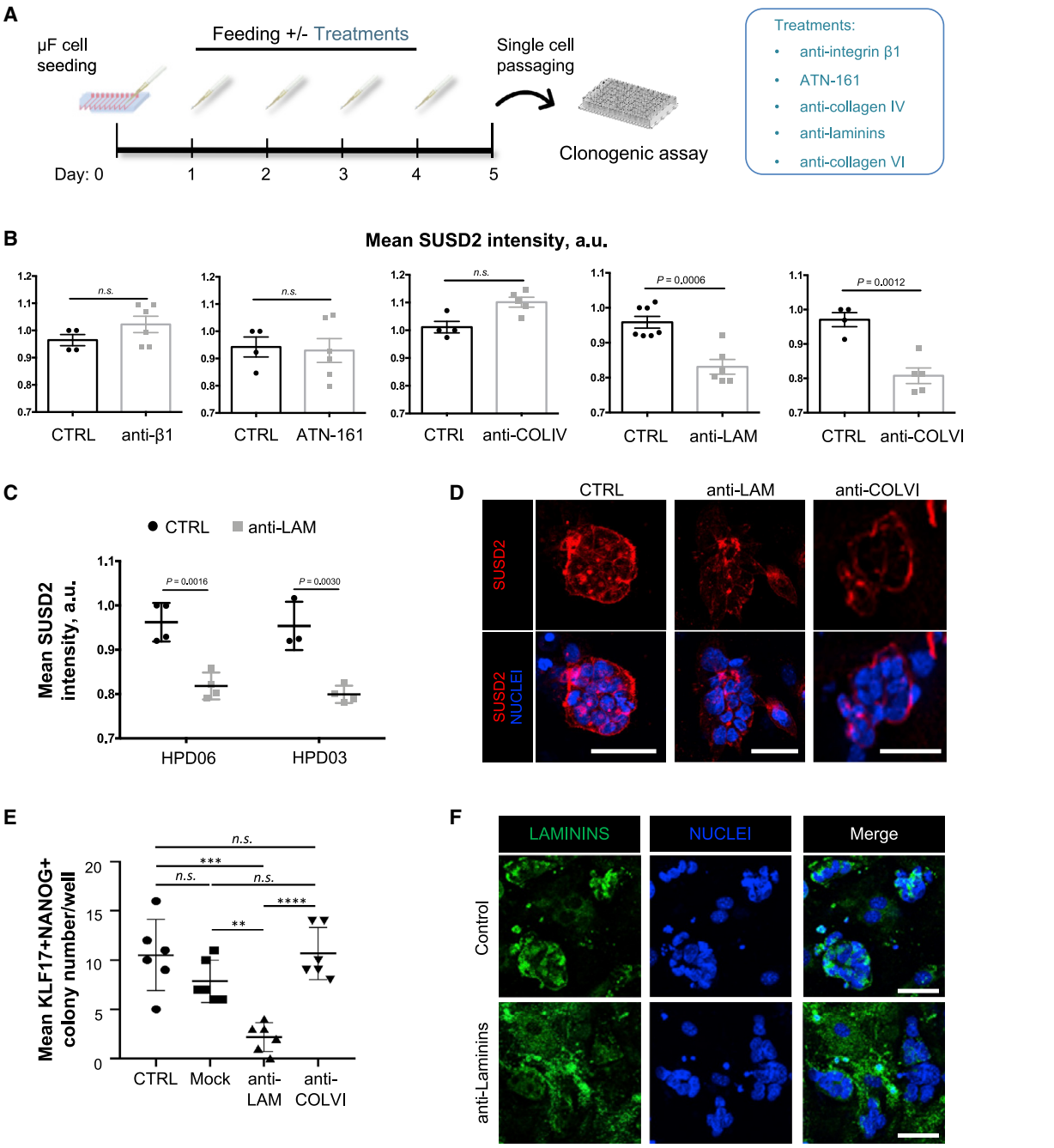

Figure 4. Disruption of naive hiPSC interaction with laminins functionally impairs the maintenance of pluripotency

(A) Experimental design: single naive hiPSCs were seeded in microfluidics on feeders. After 24 h, cells were fed either with RSeT medium (control condition) or with RSeT supplemented with antibodies against laminins, collagen type IV, collagen type VI, or Integrin β1 or with ATN161 (treatment condition, light blue). Cells were fixed at day 5 for immunofluorescence analysis and passaged as single cells to perform a clonogenicity assay.

(B) Quantification of SUSD2 mean fluorescence intensity of untreated control (CTRL), anti-integrin β1, ATN-161-, anti-laminins-, anti-collagen IV-, and anti-collagen VI-treated samples. Each dot represents an entire microfluidic channel. n = 4–7. Data are shown as mean ± SD; unequal variance Student's t test. p = 0.0006, p = 0.0012; n.s., not significant.

(C) Quantification of SUSD2 mean fluorescence intensity of untreated control and anti-laminin antibody-treated samples. Dots represent an entire microfluidic device (HPD03 cell line, left part of the graph) or entire microfluidic channels (HPD06 line, right part of the graph). n = 3–4. Data are shown as mean ± SD; unequal variance Student's t test. p = 0.0016, p = 0.0030; n.s., not significant.

(D) Representative z-stacks of naive hiPSCs cultured in microfluidics, untreated (left panels) or treated with anti-laminins (middle panels) and anti-collagen VI (right panels) antibodies. Samples were immunostained for SUSD2 (red). Nuclei were stained with Hoechst (blue). Scale bars, 50 µm.

(legend continued on next page)

be enriched around naive colonies (Figures 4 and S3G). For this set of experiments, naive hiPSCs were cultured on MEFs in microfluidics and treated for 4 days, and then quantification of SUSD2 fluorescence intensity was used as a proxy for naive pluripotency.[17] Among all the different compounds used, a significant reduction in SUSD2 fluorescence intensity was observed only for the samples treated with anti-laminins and anti-collagen type VI antibodies when compared to their relative untreated controls (Figures 4B–4D). We also observed that upon anti-laminins treatment, naive hiPSC colonies appeared visibly smaller and flatter in their morphology compared to untreated, mock-treated, and anti-collagen type VI-treated samples (Figure S3G). Therefore, we investigated whether anti-laminins and anti-collagen type VI treatments functionally impaired the maintenance of naive hiPSC pluripotency by performing a clonogenicity assay followed by staining for NANOG and KLF17. Importantly, a statistically significant reduction in the number of naive colonies was observed in anti-laminins-treated naive hiPSCs when compared to untreated, mock-treated, and anti-collagen type VI-treated cells (Figure 4E). Interestingly, anti-laminins-treated samples showed scattered and poorly organized laminins deposition in the proximity of naive hiPSCs (Figure 4F, lower panel) when compared to untreated controls (Figures 4F, upper panel, and 1E).

Overall, we showed that anti-laminin antibody treatment of naive hiPSCs reduced naive marker expression and functionally reduced the clonogenicity of the cells after only 4 days of treatment. Our data, together with reported evidence,[18] strongly suggest that laminins might have a direct role in supporting pluripotency maintenance of naive hiPSCs.

3D ECM-rich environment supports long-term feeder-free culture of naive hiPSCs

Our data demonstrate that naive hiPSCs are capable of transcribing and secreting ECM proteins and that these proteins, in particular basement membrane component laminins, are organized in a shell over the 3D colony surface (Figures 1E and 2A). Moreover, we demonstrated that by blocking the interaction of naive hiPSCs with laminins, there is a reduction in their clonogenicity (Figure 4E). Therefore, we hypothesized that the presence and 3D organization of ECM proteins may be instrumental for the robust expansion of naive hiPSCs and related to their intrinsic tendency to organize into 3D domed colonies despite culture on 2D surfaces. Thus, we functionally tested whether providing a 3D ECM-rich environment could support long-term feeder-free self-renewal of naive hiPSCs by embedding naive cells in 3D Matrigel or Geltrex, known to be rich in basement membrane components including laminins (Figure 5A).[36]

Naive hiPSCs embedded as single cells in 3D ECM-rich gels were able to survive, grow, and form 3D colonies (Figure 5B). Passaging of these colonies by single-cell dissociation and re-embedding demonstrated the long-term ability of this 3D environment to support naive hiPSC self-renewal (Figures 5C and S4A) without any overt difference in split ratio or clonogenicity compared to standard 2D MEF culture system (Figure S4B). We confirmed naive identity maintenance after 14 passages in 3D by immunostaining for KLF17, OCT4, and SUSD2 and by qRT-PCR analyses for naive (*TFCP2L1*, *KLF4*, *KLF17*, and *DPPA5*), core (*OCT4* and *NANOG*), and primed (*ZIC2)* pluripotency markers (Figures 5D, 5E, and S4C). We also confirmed that naive hiPSCs cultured in our 3D ECM-rich environment are similar to 2D-cultured naive hiPSCs through transcriptomic and principal component analyses (Figure 5F), even after prolonged passaging. At the time of submission, we have robustly expanded naive hiPSCs in 3D feeder-free culture conditions continuously for >50 passages (>250 days).

After each 3D passage, cells grew clonally, forming compact colonies without visual evidence of a lumen, as characteristic of the naive state both *in vitro* and *in vivo* (Figures 5C and S4A).[10,37,38] Immunostaining of 3D colonies revealed further details of their morphological organization, confirming the absence of lumen and confirming apolar positioning of mitotic nuclei within the compact cell mass (Figure 5G).

Pluripotent stem cells are functionally defined not only by their ability to self-renew but also by their potential to differentiate into all embryonic lineages. Additionally, human naive PSCs have recently been shown to retain the potential to differentiate into extra-embryonic lineages and are thus considered totipotent.[39–43] We confirmed that long-term 3D-cultured naive hiPSCs also maintained these functional properties, differentiating into embryonic lineages (ectoderm, mesoderm and endoderm, Figure S4D) and into extra-embryonic lineages (trophoblast stem cells, Figure S4E, and primitive endoderm, Figure S4F) when subjected to the corresponding differentiation conditions.[42,44,45]

To further confirm the totipotency of our 3D-cultured naive hiPSCs, we tested their potential to form blastoids, an *in vitro* model that mimics pre-implantation blastocysts.[46–48] We disaggregated our 3D naive colonies, then followed a protocol recently published by Yanagida and colleagues, reaggregating the cells in U-bottom wells (Figure S4G). Blastoids were generated after 4–5 days in culture, exhibiting extra-embryonic trophoblast (GATA3+) properly segregated from the naive epiblast (KLF17+) (Figure S4H).

Together, these results demonstrate robust long-term culture of naive hiPSCs in 3D, including maintenance of their identity signature, self-renewal and clonogenicity properties, morphological hallmarks, and their potency to differentiate into all embryonic and extra-embryonic lineages.

Next, we characterized ECM organization in 3D naive hiPSC cultures and blastoids by immunostaining. To allow the clear visualization of different ECM proteins, 3D colonies were cryosectioned (Figures 5H and S5A). In general, ECM protein deposition around 3D colonies was similar to that observed in 2D cultures on MEFs (Figures 1 and 2), with clear organization of collagen type IV and laminins around the colony edges, modest

(E) Clonal assay performed on naive hiPSCs previously cultured in microfluidics in RSeT (control) or in RSeT supplemented with mock, anti-laminins, or anti-collagen type VI antibodies. Scoring of double NANOG+ KLF17+ positive colonies. Data are shown as mean ± SD; one-way ANOVA with Tukey's multiple comparisons test. n = 6. p value (**) = 0.0059. p value (***) = 0.0001. p value (****) = < 0.0001.
(F) Representative z-stacks of naive hiPSCs cultured in microfluidics in RSeT (control, upper panels) or RSeT supplemented with anti-laminins antibody (lower panels). Cells were immunostained for laminins (green). Nuclei were stained with Hoechst (blue). Scale bars, 50 μm.

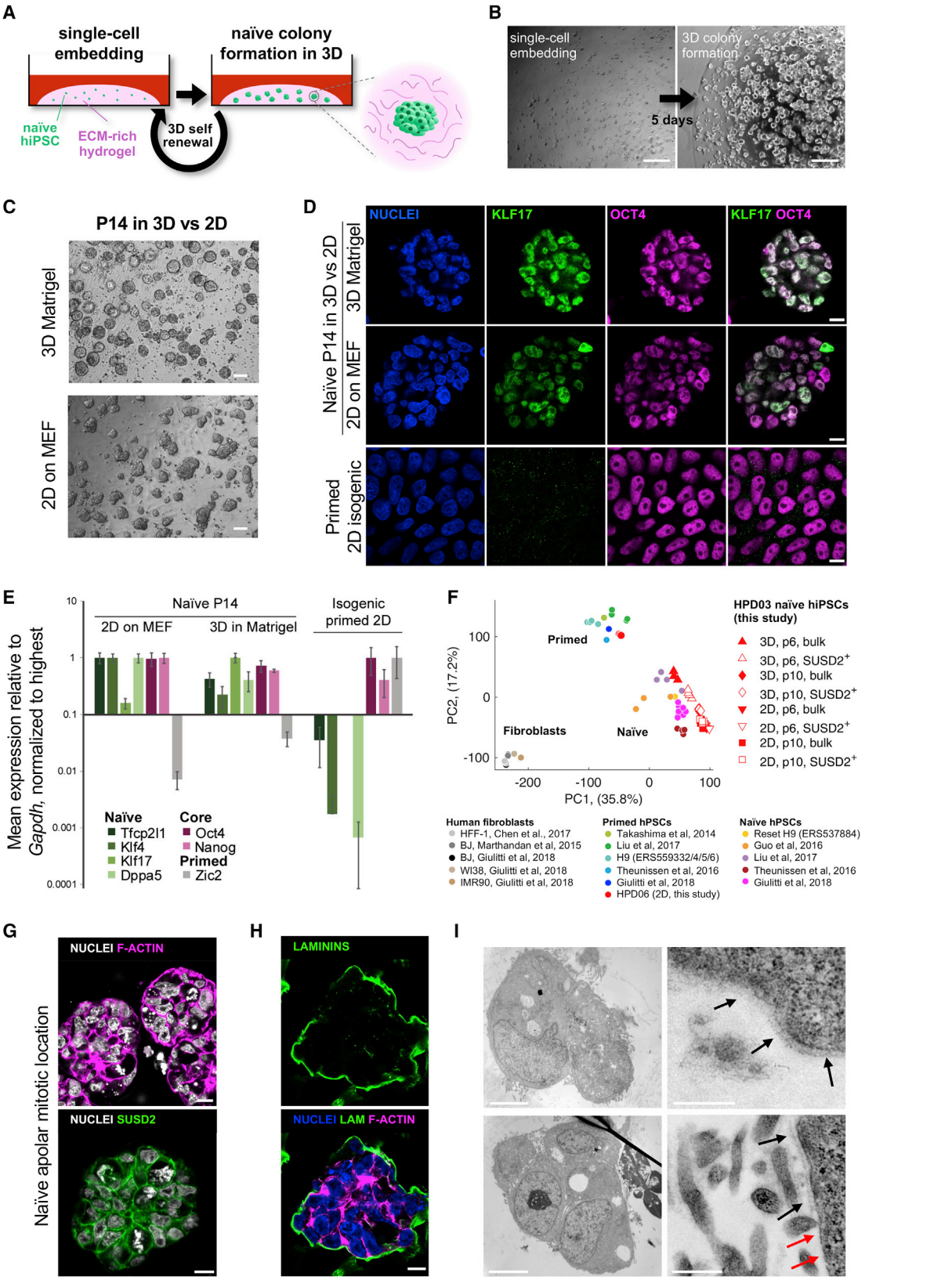

(legend on next page)

extracellular organization of collagen type I, and lack of collagen type VI in the vicinity of naive colonies (Figures 5H and S5A). We directly compared collagen type IV organization in 3D versus 2D cultures by wholemount staining. This revealed a marked layer of collagen type IV organized around naive colonies, thicker and more homogeneous in 3D compared to 2D cultures (Figures S5B and S5C), suggestive of basement membrane formation in 3D. Analysis of 3D-cultured naive hiPSCs with TEM confirmed the presence of a layer of basement membrane on the surface of the colonies (Figure 5I, black arrows). While we cannot distinguish the proportions of ECM proteins originating from the gel versus from cellular secretion, the extracellular organization of this layer must be naive-cell-autonomous given the absence of other cell types in this feeder-free culture regime.

The blastoids generated from 3D-cultured naive hiPSCs (Figures S4G and S4H) allowed us to investigate, in a model that mimics the pre-implantation blastocyst, the production and localization of ECM proteins identified in our work as secreted by naive hiPSCs (Figures 1, 2, and 3). In blastoids, we observed production and organization mainly of laminins (Figure S5D, upper panel) and some collagen type IV (Figure S5D, lower panel), whereas we did not detect collagen type I and VI (data not shown). Laminins were found within the epiblast cell cluster with a distribution like that observed in naive cultures in 3D and on MEF (Figures 5H, 1E, and S5E). In blastoids, laminins also seemed to be produced by naive-derived trophoblast cells, as revealed by the presence of the protein in correspondence with the trophoblast squamous epithelium (Figure S5F).

3D-cultured naive hiPSCs undergo timely developmental morphogenesis in response to signal cues

In vivo, naive cells do not directly enter into germ lineage differentiation.[10,49] Instead, the key function of the naive epiblast is to undergo timely identity progression from naive towards primed pluripotency as the embryo implants, with concurrent lumenogenesis and transition from an apolar cell mass into a polarized epithelium, thus preparing the post-implantation epiblast for body axis formation and gastrulation.[10,38] To challenge whether our 3D-cultured naive hiPSCs can recapitulate this coupling of identity progression with tissue morphogenesis, after 14 naive maintenance passages in 3D, we again passaged single cells into 3D as usual. However, instead of providing naive maintenance media, we stimulated them with signals to promote exit from naive state and transition towards primed pluripotent identity (Figure 6A). After 5 days in FGF2-containing medium, immunostaining showed downregulation of naive marker KLF17, upregulation of primed marker OTX2, continued expression of core pluripotency markers OCT4 and NANOG, and formation of an apical lumen within an epithelium (Figure 6B). After further culture in E8 primed media from day 5 to day 9, KLF17 expression became undetectable, while OTX2, OCT4, and NANOG expression persisted (Figures 6B and S6A), consistent with acquisition of primed pluripotent identity in a timely manner. Time course qRT-PCR analyses confirmed our immunostaining observations, demonstrating the transition of naive hiPSCs towards the primed state in 3D (Figure S6B). We confirmed that cells obtained after the 3D priming process were functionally pluripotent, with the potential to differentiate into embryonic lineages ectoderm, mesoderm, or endoderm when subjected to corresponding primed hiPSC differentiation conditions (Figure S6C).[50–52]

To characterize the gene expression dynamics of naive hiPSC priming in 3D, we performed RNA-seq at days 0, 2, 4, 6, 8, and 10 of the transition and of isogenic primed hiPSCs in 3D culture (Figures 6C, 6D, and S6D–S6G). PCA for all genes shows a clear trajectory from naive towards primed transcriptomic signature in 3D culture (Figure 6C), corroborated by an increasing number of differentially expressed genes (DEGs) relative to naive starting point and a decreasing number of DEGs relative to primed destination over time (Figure S6D). The progressive transition away from naive and towards primed signature during the time course is further supported by comparing DEG lists to assess their degree of overlap. We plotted Venn diagrams to find the numbers of DEGs relative to naive or primed reference samples that are unique to or shared between timepoints (Figure S6E). Relative to naive, the proportion of DEGs shared between a given timepoint and primed hiPSCs increased over time, indicating that 3D priming hiPSCs progressively gain differences from naive starting point that are in common with primed hiPSCs (Figure S6E).

To examine the transition dynamics in more detail, we generated a list comprising all DEGs for all pairwise comparisons between any two timepoints (11,570 total). Clustering analysis on this compiled DEGs list distinguished five major clusters,

Figure 5. 3D ECM-rich environment supports long-term self-renewal of naive hiPSCs

(A) Experimental design: single naive hiPSCs embedded in ECM-rich hydrogel drops (Matrigel or Geltrex). Colonies were passaged every 5 days.

(B) Representative bright field images showing the clonal growth of 3D naive colonies within a Matrigel drop. On the left, single cells soon after seeding, and on the right, growing colonies 5 days after seeding. Scale bars, 250 μm.

(C) Representative bright field images showing in parallel 3D (top image) and 2D (bottom image) naive hiPSC cultures after 14 passages. Scale bars, 100 μm.

(D) Representative single confocal slices of 3D naive (upper panel) and 2D naive (middle panel) after 14 passages in parallel and control 2D isogenic primed (bottom panel) hiPSCs immunostained for KLF17 (green) and OCT4 (magenta). Nuclei were stained with Hoechst (blue). Scale bars, 10 μm.

(E) qRT-PCR for naive, primed, and core pluripotency markers, normalized to *GAPDH* then to highest, displayed as mean ± SD. n = 3.

(F) PCA of naive hiPSCs (red) from 2D culture on feeders and 3D culture in Matrigel at different passage numbers (P6 and P10). Before the transcriptomic analysis, live cells (bulk) and SUSD2-positive cells (SUSD2$^+$) were sorted. Human fibroblasts, primed hiPSCs, and naive hiPSCs from this and other studies were used as controls. Names of the cell lines are reported in Table S6.

(G) Representative single confocal slices of 3D naive hiPSCs at P14 immunostained for F-actin (magenta) and naive-specific surface marker SUSD2 (green) showing apolar mitotic nuclei localization. Nuclei were stained with Hoechst (gray). Scale bars, 10 μm.

(H) Representative single confocal slice of a cryosectioned 3D naive hiPSC colony after 14 passages in Matrigel, immunostained for laminins (green) and F-actin (magenta), showing the organization of the ECM around the 3D colony. Nuclei were stained with Hoechst (blue). Scale bar, 10 μm.

(I) Representative TEM images showing 3D naive hiPSC colonies (left panels) and details of ECM organization at higher magnification (right panels). The black arrows indicate basal membrane organization at the external surface of cell aggregates. Red arrows indicate discontinuity in the basal membrane layer. Scale bars of left panels, 5 μm; right panels, 500 nm.

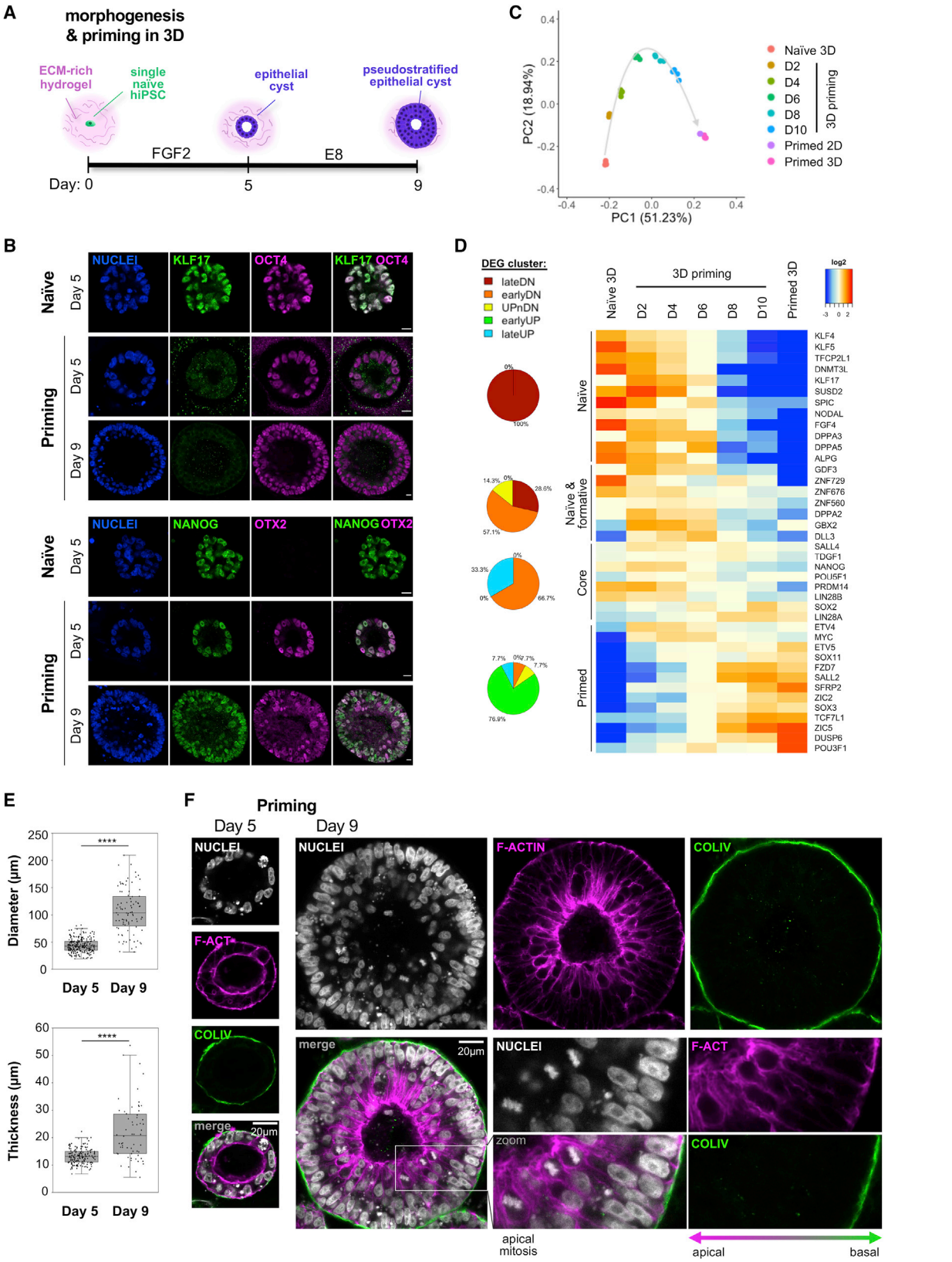

(legend on next page)

identified by minimizing total variation within each cluster: 1, late down (868); 2, early down (4,455); 3, up-then-down (928); 4, early up (1,334); and 5, late up (3,985) (Figure S6F). We compiled gene lists characteristic of the naive-to-primed transition from KEGG pathways and published literature,[44,49,53] plotted their expression in heatmaps, and examined the contribution of each cluster to their dynamics (Figures 6D and S6G). The majority of genes related to naive pluripotency (100%) and shared between naive and formative pluripotency (86%) are downregulated (clusters 1 and 2), with the exception of GBX2 and DLL3 that show the expected up-then-down (cluster 3) profile associated with the transition from naive through formative pluripotency in the primate embryo (Figure 6D).[49] In contrast, genes related to primed pluripotency mostly fit to upregulated clusters (85%, clusters 4 and 5), while core pluripotency genes are expressed throughout, either not classifying as DEGs (e.g., SALL4 and TDGF1) or fitting to DEG clusters with least steep rates of change (2 and 5) (Figure 6D). We noted that genes related to oxidative phosphorylation are mostly downregulated (75%, clusters 1 and 2), whereas those associated with glycolysis are mostly upregulated (70%, clusters 4 and 5), consistent with the expected metabolic switch from naive to primed pluripotency (Figure S6G). Interestingly, genes related to tight junctions, cell polarity, integrins, and cadherins were predominant in the upregulated clusters (Figure S6G), suggestive of changes in tissue architecture such as epithelialization and lumenogenesis concomitant with the naive-to-primed identity transition. Indeed, by immunofluorescence we observe a dynamic overlap of morphogenetic changes and lumenogenesis during the priming transition from naive hiPSCs in a 3D environment (Figures 6B, 6E, and 6F).

Morphologically, by day 9, the 3D epithelial cysts formed during priming in 3D from single naive hiPSCs developed into pseudostratified epithelia with correct apical-basal geometry (Figures 6B, 6E, and 6F). This corresponded with a growth in cyst diameter from day 5 to day 9 and an increase in thickness of the epithelial layer (Figure 6E). On day 9, mitotic nuclei were found at the F-Actin-rich apical domain adjacent to the lumen, whereas the majority of other nuclei were aligned around the basal edge adjacent to the well-organized collagen type IV indicative of basement membrane (Figure 6F). The stratification index of day 9 epithelia was between 2 and 3 (i.e., 2–3 rows of nuclei). The dramatic increase in cyst size from day 5 to day 9 (Figures 6E and 6F, images presented at identical scale) suggests rapid remodeling of the collagen type IV layer to accommodate growth.

In sum, these data show that culture in a 3D ECM-rich environment supports single naive hiPSCs to undergo both long-term self-renewal and timely developmental morphogenesis in response to signaling cues.

DISCUSSION

Growth in compact, dome-shaped colonies is considered a hallmark of naive hiPSCs, acknowledging their characteristic tendency to form 3D colonies despite the conventionally used 2D culture platforms. Interestingly, we found that the surface of these domed colonies is covered by a layer of ECM proteins that outlines their characteristic shape. While substantial efforts have been made to unravel the cell signaling pathways supporting naive hiPSC self-renewal, until now little consideration has been given to characterization of the ECM in their colony environment and its role in naive hiPSC identity maintenance.

Our results show that naive hiPSCs in standard 2D *in vitro* culture express and produce ECM proteins, which are organized in the cellular microenvironment as the colony forms and grows. We observed that some of these proteins, which are also components of *in vivo* basement membranes like collagen type IV and laminins, are deposited and organized on the surface of naive colonies, forming a "coat-like" layer that outlines the characteristic dome shape of naive colonies.

By integrating microfluidic, proteomic, and transcriptomic technologies, we were able to identify ECM species transcribed, translated, and secreted by naive hiPSCs and/or their supporting MEF feeder layer. We concluded that MEF-only cultures express proteins involved in ECM organization, which can contribute to the increased deposition of some ECM proteins observed when hiPSCs are cultured on feeders (Figures 1E, 1F, and 2A). Whether this MEF contribution in ECM protein production and remodeling affects naive cell maintenance in 2D *in vitro* cultures is still an open question. To date, feeder-free naive culture conditions have been reported in only a few works,[18,19,24] and in these 2D systems, the addition of large amounts of ECM proteins like laminins or gel mixtures was necessary. Starting from these

Figure 6. 3D ECM-rich environment supports developmental morphogenesis of naive hiPSCs

(A) Experimental design: single naive hiPSCs embedded in Matrigel drops were induced to exit from the naive state. Cells were fixed at day 5 and day 9 for immunofluorescence characterization of pluripotent identity and morphogenesis.

(B) Panels showing identity transition in the 3D environment. In the left panel, representative single confocal slices of day 5 3D naive (left), day 5 priming (middle), and day 9 3D priming (right) immunostained for KLF17 (green) and OCT4 (magenta). In the right panel, representative single confocal slices of the same conditions immunostained for OTX2 (magenta) and NANOG (green). Nuclei were stained with Hoechst (blue). Scale bars, 10 μm.

(C) PCA of bulk RNA-seq of 3D naive hiPSCs, naive hiPSCs at days 2, 4, 6, 8, and 10 days of priming in 3D, and isogenic 2D and 3D primed showing the trajectory (gray arrow) of cell identity transition.

(D) Heatmap showing the median-centered expression of selected genes, ordered by their belonging to the clusters shown in Figure S6F. The related pie charts represent the percentage of genes that belong to each of clusters 1–5. Only DEGs are presented, except for SALL4 and TDGF1 that did not meet the thresholds to be assigned as differentially expressed, but are presented since they are informative markers of core pluripotent identity. Gene lists were compiled from KEGG pathways and published literature.[44,49,53]

(E) Boxplots of mean diameter and mean epithelial thickness for day 5 and day 9 cysts. Each dot represents a cyst. 224 (day 5) and 89 (day 9) cysts counted across 3 20× confocal images from three technical replicates (diameter). 161 (day 5) and 60 (day 9) cysts counted across 3 20× confocal images from two technical replicates (thickness). Unequal variance Student's t test, p (****) < 0.0001.

(F) Representative single confocal slices of day 5 3D priming (left panel) and day 9 3D priming (right panel) immunostained for F-actin (magenta) and collagen type IV (COLIV, green), showing the morphological process of lumenogenesis and epithelialization. Nuclei were stained with Hoechst (gray). Day 5 and day 9 images are presented at the same scale to appreciate cyst growth. Scale bars, 20 μm.

considerations and our observations regarding the presence of ECM proteins around the domed naive colony microenvironment and the requirement of deposited laminins for hiPSC clonogenicity (Figure 4), we tested whether 3D provision of exogenous ECM components could sustain naive identity.

Our work shows that encapsulation in 3D hydrogels rich in basement-membrane components supports robust feeder-free naive hiPSC culture over many passages (>50 so far). As well as maintenance of naive identity signature and morphology, functional characteristics such as clonal self-renewal or multilineage embryonic and extra-embryonic differentiation potential are preserved. During 3D naive colony growth, collagen type IV and laminins are strongly organized around the colonies. While these basement membrane proteins likely originate from the gel as well as possibly from naive cellular production, it will be of future interest to understand how the naive cells themselves direct ECM remodeling around the colonies. The omics data reported in this manuscript, including proteomics of naive hiPSC secretome, constitute a valuable community resource, opening a window into future identification of candidate mechanisms for how naive hiPSCs sculpt their microenvironment.

Within the same 3D ECM-rich environment, we demonstrate that single naive hiPSCs can be directed to undergo identity transition towards primed state, coupled with lumenogenesis and tissue morphogenesis into pseudostratified epithelium. Often, *in vitro* stem cell differentiation protocols entail transfer from a maintenance platform into a different environment; an artificially abrupt change compared to the embryo, which progresses continually along its developmental trajectory. In contrast, we show that the same 3D ECM-rich environment supports both naive hiPSC self-renewal and developmental identity progression, i.e., both critical aspects of naive stem cell functionality. We speculate that this may be due to the more embryo-typic niche provided: the strong 3D organization of collagen type IV we observe is reminiscent of the basement membrane experienced between the embryonic epiblast and primitive endoderm *in vivo*.[12] In the future, it will be interesting to compare the gene regulatory network and epigenetic transitions between 2D versus 3D naive state exit and onward development, both in terms of the sequence and tempo of events, and to compare which one better matches embryonic processes.

Consistent with our observation, the tendency of naive human PSCs to undergo lumenogenesis in response to priming signals in 3D has been reported recently.[38] There, after 48 h exposed to priming signals, Shahbazi and colleagues observed apical domain formation and initiation of lumenogenesis. Here, we take this further: after 5 days we reach the formation of a large lumen (Figure 6F, left panel), then by day 9 the surrounding epithelium has grown remarkably, thickening and becoming pseudostratified (Figures 6E and 6F, right panel). This shows an advanced degree of 3D morphogenesis occurring directly from a single naive hiPSC. Meanwhile, the dramatic increase we observe in cyst size, and the corresponding increase in diameter of the basal collagen type IV layer from days 5–9 (Figures 6E and 6F), forms an intriguing parallel with a recent report[11] that basement membrane remodeling is critical during mouse embryonic growth and morphogenesis during the naive-to-primed transition.

Our findings open the realistic possibility of modeling key stages of human development in 3D starting from a single cell. The clonal nature of our system, in contrast to strategies involving aggregation of 100s–1,000s of primed hiPSCs, may permit the study of symmetry breaking and tissue patterning unconfounded by pre-existing heterogeneity. Starting from the naive state, we may also gain access to earlier state transitions relevant for healthy human embryogenesis during the critical period of implantation. Intriguingly, recent reports suggest that, unlike mouse naive PSCs, human naive PSCs have not yet restricted access to extra-embryonic primitive endoderm[42] and trophectoderm[43] lineages, at least at the population level. Our clonal 3D system for developmental morphogenesis from a single naive hiPSC offers the fascinating future possibility to challenge whether a single naive hiPSC does indeed possess the totipotency to form all embryonic and extra-embryonic lineages and to challenge to what extent their spatial self-organization is an intrinsic, regulative property.

Limitations of the study

Although we used commercially available ECM-rich hydrogels, which represent the gold standard for organoid 3D cultures (Matrigel or Geltrex), we are aware that these products are extracted from tissues and are thus neither synthetic nor chemically defined. Indeed, they show some degree of batch-to-batch variability that must be kept in mind when standardizing 3D naive hiPSC culture. The undefined nature of Matrigel or Geltrex also challenged our ability to dissect which specific ECM-associated cellular interactions and ECM downstream signaling pathways are instrumental for supporting the naive state of pluripotency and the mechanism by which this is achieved. Further advances toward chemically and mechanically defined synthetic hydrogels remain a future goal to fully unlock naive hiPSC potential ranging from developmental and disease modeling to translational applications.

STAR★METHODS

Detailed methods are provided in the online version of this paper and include the following:

- KEY RESOURCES TABLE
- RESOURCE AVAILABILITY
  - Lead contact
  - Materials availability
  - Data and code availability
- EXPERIMENTAL MODEL AND SUBJECT DETAILS
  - Cell lines
  - Cell culture in 2D
  - Cell short-term cultures in microfluidic devices
  - Cell expansion in 3D
- METHOD DETAILS
  - ECM treatments and clonogenicity assay
  - Naive to primed conversion in 2D
  - Naive to primed conversion in 3D
  - Extra-embryonic multilineage differentiation in 2D
  - Multilineage differentiation in 2D
  - Blastoid generation
  - Electron microscopy imaging
  - Immunohistochemistry
  - Imaging analysis and quantification

- RNA sequencing and transcriptomic analysis
- Quantitative reverse transcriptase PCR
- Conditioned medium, total lysates and decellularization for proteomic analysis
- Proteomic sample pre-processing
- Proteomic bioinformatics analysis

- QUANTIFICATION AND STATISTICAL ANALYSIS

SUPPLEMENTAL INFORMATION

Supplemental information can be found online at https://doi.org/10.1016/j.stem.2022.11.011.

ACKNOWLEDGMENTS

We are grateful to SIAIS Analytical Platform (Dr. Wenzhang Chen and Dr. Wei Zhu) at ShanghaiTech University for mass spectrometry analyses. We thank the support of TIGEM NGS and Bioinformatics Cores and Next Generation Diagnostic srl. We thank Prof. Faessler Reinhard, Prof. Beate Eckes, and Prof. Paolo Bonaldo for scientific advice and discussion on ECM treatments. We are grateful to Elly Tanaka for advice and training in 3D culture methodologies. A.U. was supported by STARS Starting Grant 2017 of University of Padova (LS3-19613) and by Bando Direzione Scientifica IRP Città della Speranza (21/05). H.S. was supported by a Wellcome Trust Sir Henry Wellcome postdoctoral fellowship. C. Luni was supported by the Natural Science Foundation of China (31601178). C. Laterza was supported by Marie Curie Individual fellowship (839753). O.G. was supported by University of Padova under the 2019 STARS Grants program (iNeurons) and Fondazione Umberto Veronesi fellowship. G.M.'s laboratory is supported by grants from the Giovanni Armenise–Harvard Foundation, the Telethon Foundation, and an ERC Starting Grant (MetEpiStem). C. Luni, S.M., M.C., and N.E. were supported by grant F-0301-15-009 by ShanghaiTech University. N.E. and H.S. acknowledge the support of the NIHR GOSH BRC. This work was supported by Fondazione Telethon Core Grant, Armenise-Harvard Foundation Career Development Award, European Research Council (grant agreement 759154, CellKarma), and the Rita-Levi Montalcini program from MIUR to D.C. This work was supported by 2018 STARS-WiC grant of University of Padova, Progetti di Eccellenza CaRiPaRo, TWINING of University of Padova, and the Oak Foundation Award (Grant No. W1095/OCAY-14-191) to N.E.

AUTHOR CONTRIBUTIONS

E.C., A.U., H.S., and N.E. designed the experiments. A.U., E.T., and E.C. performed and analyzed ECM experiments. H.S. and E.C. performed 3D experiments. P.S. and S.Q. performed electron microscopy and analysis. I.Z. and G.M. helped in establishing naive hiPSC culture conditions in 2D. R.M.B. performed 2D differentiation and qRT-PCR analysis of trophoblast stem cells from 3D naive hiPSCs. C. Laterza performed and analyzed 2D naive to primed conversion. O.G. optimized naive hiPSC culture condition in 2D microfluidics and helped analyze the data. C. Luni helped in designing the proteomic and RNA-seq experiment. A.M., L.D., and D.C. performed RNA-sequencing. A.G., L.D., and C. Luni performed RNA-seq bioinformatic analyses. S.M. and M.C. performed proteomic sample preparation. C. Luni performed proteomic bioinformatic analyses and helped write the manuscript. E.C., A.U., H.S., and N.E. wrote the manuscript. N.E. supervised the project.

DECLARATION OF INTERESTS

D.C. is founder, shareholder, and consultant of Next Generation Diagnostic srl. A.M. and L.D. are employees of Next Generation Diagnostic srl.

Received: December 22, 2020
Revised: February 7, 2022
Accepted: November 9, 2022
Published: December 1, 2022

REFERENCES

1. Chen, K., Mallon, B., McKay, R., and Robey, P. (2014). Human pluripotent stem cell culture: Considerations for maintenance, expansion, and therapeutics. Cell Stem Cell *14*, 13–26. https://doi.org/10.1016/j.stem.2013.12.005.
2. Weinberger, L., Ayyash, M., Novershtern, N., and Hanna, J.H. (2016). Dynamic stem cell states: naive to primed pluripotency in rodents and humans. 2016. Nat. Rev. Mol. Cell Biol. *17*, 155–169. https://doi.org/10.1038/nrm.2015.28.
3. Morgani, S., Nichols, J., and Hadjantonakis, A.-K. (2017). The many faces of Pluripotency: in vitro adaptations of a continuum of in vivo states. BMC Dev. Biol. *17*, 7. https://doi.org/10.1186/s12861-017-0150-4.
4. Stirparo, G.G., Boroviak, T., Guo, G., Nichols, J., Smith, A., and Bertone, P. (2018). Integrated Analysis of Single-Cell Embryo Data Yields a Unified Transcriptome Signature for the Human Pre-implantation Epiblast. Development *145*. Cambridge.
5. Dong, C., Fischer, L.A., and Theunissen, T.W. (2019). Recent insights into the naïve state of human pluripotency and its applications. Exp. Cell Res. *385*, 111645. https://doi.org/10.1016/j.yexcr.2019.111645.
6. Rossant, J., and Tam, P.P. (2017). New Insights into Early Human Development: Lessons for Stem Cell Derivation and Differentiation. Cell Stem Cell *20*, 18–28. https://doi.org/10.1016/j.stem.2016.12.004.
7. Boroviak, T., and Nichols, J. (2017). Primate embryogenesis predicts the hallmarks of human naïve pluripotency. Development (Camb.) *144*, 175–186. https://doi.org/10.1242/dev.145177.
8. Geng, T., Zhang, D., and Jiang, W. (2019). Epigenetic Regulation of Transition Among Different Pluripotent States: Concise Review. Stem Cell. *37*, 1372–1380. https://doi.org/10.1002/stem.3064.
9. Theunissen, T., Friedli, M., He, Y., Planet, E., O'Neil, R., Markoulaki, S., Pontis, J., Wang, H., Iouranova, A., Imbeault, M., et al. (2016). Molecular Criteria for Defining the Naive Human Pluripotent State. Cell Stem Cell *19*, 502–515. https://doi.org/10.1016/j.stem.2016.06.011.
10. Shahbazi, M.N. (2020). Mechanisms of Human Embryo Development: From Cell Fate to Tissue Shape and Back. Development *147*. Cambridge.
11. Kyprianou, C., Christodoulou, N., Hamilton, R.S., Nahaboo, W., Boomgaard, D.S., Amadei, G., Migeotte, I., and Zernicka-Goetz, M. (2020). Basement membrane remodelling regulates mouse embryogenesis. 2020. Nature *582*, 253–258. 7811. https://doi.org/10.1038/s41586-020-2264-2.
12. Xiang, L., Yin, Y., Zheng, Y., Ma, Y., Li, Y., Zhao, Z., Guo, J., Ai, Z., Niu, Y., Duan, K., et al. (2020). A developmental landscape of 3D-cultured human pre-gastrulation embryos. Nature *577*, 537–542. https://doi.org/10.1038/s41586-019-1875-y.
13. Taei, A., Rasooli, P., Braun, T., Hassani, S.N., and Baharvand, H. (2020). Signal regulators of human naïve pluripotency. Exp. Cell Res. *389*, 111924. https://doi.org/10.1016/j.yexcr.2020.111924.
14. Nichols, J., and Smith, A. (2012). Pluripotency in the embryo and in culture. Cold Spring Harb Perspect Biol *4*, a008128. https://doi.org/10.1101/cshperspect.a008128.
15. Boroviak, T., Loos, R., Bertone, P., Smith, A., and Nichols, J. (2014). The ability of inner-cell-mass cells to self-renew as embryonic stem cells is acquired following epiblast specification. 2014. Nat. Cell Biol. *16*, 513–525. https://doi.org/10.1038/ncb2965.
16. Nakamura, T., Okamoto, I., Sasaki, K., Yabuta, Y., Iwatani, C., Tsuchiya, H., Seita, Y., Nakamura, S., Yamamoto, T., and Saitou, M. (2016). A developmental coordinate of pluripotency among mice, monkeys and humans. 2016. Nature *537*, 57–62. 7618. https://doi.org/10.1038/nature19096.
17. Bredenkamp, N., Stirparo, G.G., Nichols, J., Smith, A., and Guo, G. (2019). The Cell-Surface Marker Sushi Containing Domain 2 Facilitates Establishment of Human Naive Pluripotent Stem Cells. Stem Cell Rep. *12*, 1212–1222. https://doi.org/10.1016/j.stemcr.2019.03.014.
18. Guo, G., von Meyenn, F., Rostovskaya, M., Clarke, J., Dietmann, S., Baker, D., Sahakyan, A., Myers, S., Bertone, P., Reik, W., et al. (2017).

Epigenetic resetting of human pluripotency. Development (Camb.) *144*, 2748–2763. https://doi.org/10.1242/dev.146811.

19. Takashima, Y., Guo, G., Loos, R., Nichols, J., Ficz, G., Krueger, F., Oxley, D., Santos, F., Clarke, J., Mansfield, W., et al. (2014). Resetting transcription factor control circuitry toward ground-state pluripotency in human. Cell *158*, 1254–1269. https://doi.org/10.1016/j.cell.2014.08.029.
20. Theunissen, T., Powell, B., Wang, H., Mitalipova, M., Faddah, D., Reddy, J., Fan, Z., Maetzel, D., Ganz, K., Shi, L., et al. (2014). Systematic identification of culture conditions for induction and maintenance of naive human pluripotency. Cell Stem Cell *15*, 471–487. https://doi.org/10.1016/j.stem.2014.07.002.
21. Soteriou, D., Iskender, B., Byron, A., Humphries, J.D., Borg-Bartolo, S., Haddock, M.C., Baxter, M.A., Knight, D., Humphries, M.J., and Kimber, S.J. (2013). Comparative proteomic analysis of supportive and unsupportive extracellular matrix substrates for human embryonic stem cell maintenance. J. Biol. Chem. *288*, 18716–18731. https://doi.org/10.1074/jbc.m113.463372.
22. Xu, C., Inokuma, M.S., Denham, J., Golds, K., Kundu, P., Gold, J.D., and Carpenter, M.K. (2001). Feeder-free growth of undifferentiated human embryonic stem cells. Nat. Biotechnol. *19*, 971–974. https://doi.org/10.1038/nbt1001-971.
23. Braam, S.R., Zeinstra, L., Litjens, S., Ward-van Oostwaard, D., van den Brink, S., van Laake, L., Lebrin, F., Kats, P., Hochstenbach, R., Passier, R., et al. (2008). Recombinant Vitronectin Is a Functionally Defined Substrate That Supports Human Embryonic Stem Cell Self-Renewal via αVβ5 Integrin. Stem Cell. *26*, 2257–2265. https://doi.org/10.1634/stemcells.2008-0291.
24. Szczerbinska, I., Gonzales, K.A.U., Cukuroglu, E., Ramli, M.N.B., Lee, B.P.G., Tan, C.P., Wong, C.K., Rancati, G.I., Liang, H., Göke, J., et al. (2019). A Chemically Defined Feeder-free System for the Establishment and Maintenance of the Human Naive Pluripotent State. Stem Cell Rep. *13*, 612–626. https://doi.org/10.1016/j.stemcr.2019.08.005.
25. Gagliano, O., Elvassore, N., and Luni, C. (2016). Microfluidic technology enhances the potential of human pluripotent stem cells. Biochem. Biophys. Res. Commun. *473*, 683–687. https://doi.org/10.1016/j.bbrc.2015.12.058.
26. Gagliano, O., Luni, C., Qin, W., Bertin, E., Torchio, E., Galvanin, S., Urciuolo, A., and Elvassore, N. (2019). Microfluidic reprogramming to pluripotency of human somatic cells. Nat. Protoc. *14*, 722–737. https://doi.org/10.1038/s41596-018-0108-4.
27. Giobbe, G.G., Michielin, F., Luni, C., Giulitti, S., Martewicz, S., Dupont, S., Floreani, A., and Elvassore, N. (2015). Functional differentiation of human pluripotent stem cells on a chip. Nat. Methods *12*, 637–640. https://doi.org/10.1038/nmeth.3411.
28. Luni, C., Giulitti, S., Serena, E., Ferrari, L., Zambon, A., Gagliano, O., Giobbe, G.G., Michielin, F., Knöbel, S., Bosio, A., and Elvassore, N. (2016). High-efficiency cellular reprogramming with microfluidics. Nat. Methods *13*, 446–452. https://doi.org/10.1038/nmeth.3832.
29. Frantz, C., Stewart, K.M., and Weaver, V.M. (2010). The extracellular matrix at a glance. J. Cell Sci. *123*, 4195–4200. https://doi.org/10.1242/jcs.023820.
30. Groulx, J.F., Gagné, D., Benoit, Y.D., Martel, D., Basora, N., and Beaulieu, J.F. (2011). Collagen VI is a basement membrane component that regulates epithelial cell-fibronectin interactions. Matrix Biol. *30*, 195–206. https://doi.org/10.1016/j.matbio.2011.03.002.
31. Hynes, R.O., and Naba, A. (2012). Overview of the matrisome-An inventory of extracellular matrix constituents and functions. Cold Spring Harb Perspect Biol *4*, a004903. https://doi.org/10.1101/cshperspect.a004903.
32. Molè, M.A., Weberling, A., Fässler, R., Campbell, A., Fishel, S., and Zernicka-Goetz, M. (2021). Integrin β1 coordinates survival and morphogenesis of the embryonic lineage upon implantation and pluripotency transition. Cell Rep. *34*, 108834. https://doi.org/10.1016/j.celrep.2021.108834.
33. Beddingfield, B.J., Iwanaga, N., Chapagain, P.P., Zheng, W., Roy, C.J., Hu, T.Y., Kolls, J.K., and Bix, G.J. (2021). The Integrin Binding Peptide, ATN-161, as a Novel Therapy for SARS-CoV-2 Infection. JACC Basic Transl Sci *6*, 1–8. https://doi.org/10.1016/j.jacbts.2020.10.003.
34. Edwards, D.N., Salmeron, K., Lukins, D.E., Trout, A.L., Fraser, J.F., and Bix, G.J. (2020). Integrin α5β1 inhibition by ATN-161 reduces neuroinflammation and is neuroprotective in ischemic stroke. J. Cerebr. Blood Flow Metabol. *40*, 1695–1708. https://doi.org/10.1177/0271678x19880161.
35. Doñate, F., Parry, G.C., Shaked, Y., Hensley, H., Guan, X., Beck, I., Tel-Tsur, Z., Plunkett, M.L., Manuia, M., Shaw, D.E., et al. (2008). Pharmacology of the Novel Antiangiogenic Peptide ATN-161 (Ac-PHSCN-NH2): Observation of a U-Shaped Dose-Response Curve in Several Preclinical Models of Angiogenesis and Tumor Growth. Clin. Cancer Res. *14*, 2137–2144. https://doi.org/10.1158/1078-0432.ccr-07-4530.
36. Hughes, C.S., Postovit, L.M., and Lajoie, G.A. (2010). Matrigel: A complex protein mixture required for optimal growth of cell culture. Proteomics *10*, 1886–1890. https://doi.org/10.1002/pmic.200900758.
37. Shahbazi, M.N., and Zernicka-Goetz, M. (2018). Deconstructing and reconstructing the mouse and human early embryo. 2018. Nat. Cell Biol. *20*, 878–887. https://doi.org/10.1038/s41556-018-0144-x.
38. Shahbazi, M.N., Scialdone, A., Skorupska, N., Weberling, A., Recher, G., Zhu, M., Jedrusik, A., Devito, L.G., Noli, L., MacAulay, I.C., et al. (2017). Pluripotent state transitions coordinate morphogenesis in mouse and human embryos. 2017. Nature *552*, 239–243. 7684 552. https://doi.org/10.1038/nature24675.
39. Cinkornpumin, J.K., Kwon, S.Y., Guo, Y., Hossain, I., Sirois, J., Russett, C.S., Tseng, H.W., Okae, H., Arima, T., Duchaine, T.F., et al. (2020). Naive Human Embryonic Stem Cells Can Give Rise to Cells with a Trophoblast-like Transcriptome and Methylome. Stem Cell Rep. *15*, 198–213. https://doi.org/10.1016/j.stemcr.2020.06.003.
40. Dong, C., Beltcheva, M., Gontarz, P., Zhang, B., Popli, P., Fischer, L.A., Khan, S.A., Park, K.M., Yoon, E.J., Xing, X., et al. (2020). Derivation of trophoblast stem cells from naïve human pluripotent stem cells. Elife *9*, e52504. https://doi.org/10.7554/elife.52504.
41. Io, S., Kabata, M., Iemura, Y., Semi, K., Morone, N., Minagawa, A., Wang, B., Okamoto, I., Nakamura, T., Kojima, Y., et al. (2021). Capturing human trophoblast development with naive pluripotent stem cells in vitro. Cell Stem Cell *28*, 1023–1039.e13. e13. https://doi.org/10.1016/j.stem.2021.03.013.
42. Linneberg-Agerholm, M., Wong, Y.F., Herrera, J.A.R., Monteiro, R.S., Anderson, K.G.V., and Brickman, J.M. (2019). Naïve human pluripotent stem cells respond to Wnt, Nodal and LIF signalling to produce expandable naïve extra-embryonic endoderm. Development *146*. Cambridge.
43. Guo, G., Stirparo, G.G., Strawbridge, S.E., Spindlow, D., Yang, J., Clarke, J., Dattani, A., Yanagida, A., Li, M.A., Myers, S., et al. (2021). Human naive epiblast cells possess unrestricted lineage potential. Cell Stem Cell *28*, 1040–1056.e6. e6. https://doi.org/10.1016/j.stem.2021.02.025.
44. Giulitti, S., Pellegrini, M., Zorzan, I., Martini, P., Gagliano, O., Mutarelli, M., Ziller, M.J., Cacchiarelli, D., Romualdi, C., Elvassore, N., and Martello, G. (2018). Direct generation of human naive induced pluripotent stem cells from somatic cells in microfluidics. Nat. Cell Biol. *21*, 275–286. https://doi.org/10.1038/s41556-018-0254-5.
45. Okae, H., Toh, H., Sato, T., Hiura, H., Takahashi, S., Shirane, K., Kabayama, Y., Suyama, M., Sasaki, H., and Arima, T. (2018). Derivation of Human Trophoblast Stem Cells. Cell Stem Cell *22*, 50–63.e6. e6. https://doi.org/10.1016/j.stem.2017.11.004.
46. Kagawa, H., Javali, A., Khoei, H.H., Sommer, T.M., Sestini, G., Novatchkova, M., Scholte op Reimer, Y., Castel, G., Bruneau, A., Maenhoudt, N., et al. (2021). Human blastoids model blastocyst development and implantation. 2021. Nature *601*, 600–605. 7894. https://doi.org/10.1038/s41586-021-04267-8.
47. Yu, L., Wei, Y., Duan, J., Schmitz, D.A., Sakurai, M., Wang, L., Wang, K., Zhao, S., Hon, G.C., and Wu, J. (2021). Blastocyst-like structures generated from human pluripotent stem cells. 2021. Nature *591*, 620–626. 7851. https://doi.org/10.1038/s41586-021-03356-y.

48. Yanagida, A., Spindlow, D., Nichols, J., Dattani, A., Smith, A., and Guo, G. (2021). Naive stem cell blastocyst model captures human embryo lineage segregation. Cell Stem Cell *28*, 1016–1022.e4. e4. https://doi.org/10.1016/j.stem.2021.04.031.

49. Rostovskaya, M., Stirparo, G.G., and Smith, A. (2019). Capacitation of Human Naïve Pluripotent Stem Cells for Multi-Lineage Differentiation. Development *146*.

50. Chambers, S.M., Qi, Y., Mica, Y., Lee, G., Zhang, X.J., Niu, L., Bilsland, J., Cao, L., Stevens, E., Whiting, P., et al. (2012). Combined small molecule inhibition accelerates developmental timing and converts human pluripotent stem cells into nociceptors. Nat. Biotechnol. *30*, 715–720. https://doi.org/10.1038/nbt.2249.

51. Chal, J., al Tanoury, Z., Hestin, M., Gobert, B., Aivio, S., Hick, A., Cherrier, T., Nesmith, A.P., Parker, K.K., and Pourquié, O. (2016). Generation of human muscle fibers and satellite-like cells from human pluripotent stem cells in vitro. 2016. Nat. Protoc. *11*, 1833–1850. https://doi.org/10.1038/nprot.2016.110.

52. Loh, K., Ang, L., Zhang, J., Kumar, V., Ang, J., Auyeong, J., Lee, K., Choo, S., Lim, C., Nichane, M., et al. (2014). Efficient endoderm induction from human pluripotent stem cells by logically directing signals controlling lineage bifurcations. Cell Stem Cell *14*, 237–252. https://doi.org/10.1016/j.stem.2013.12.007.

53. Kinoshita, M., Barber, M., Mansfield, W., Cui, Y., Spindlow, D., Stirparo, G.G., Dietmann, S., Nichols, J., and Smith, A. (2021). Capture of Mouse and Human Stem Cells with Features of Formative Pluripotency. Cell Stem Cell *28*, 2180. e8. https://doi.org/10.1016/j.stem.2021.11.002.

54. Wiśniewski, J.R., Zougman, A., Nagaraj, N., and Mann, M. (2009). Universal sample preparation method for proteome analysis. Nat. Methods *6*, 359–362. https://doi.org/10.1038/nmeth.1322.

55. Zamir, E.A., Rongish, B.J., and Little, C.D. (2008). The ECM Moves during Primitive Streak Formation—Computation of ECM Versus Cellular Motion. PLoS Biol. *6*, e247. https://doi.org/10.1371/journal.pbio.0060247.

56. Truckenbrodt, S., Viplav, A., Jähne, S., Vogts, A., Denker, A., Wildhagen, H., Fornasiero, E.F., and Rizzoli, S.O. (2018). Newly produced synaptic vesicle proteins are preferentially used in synaptic transmission. EMBO J. *37*, e98044. https://doi.org/10.15252/embj.201798044.

57. Dankovich, T.M., Kaushik, R., Olsthoorn, L.H.M., Petersen, G.C., Giro, P.E., Kluever, V., Agüi-Gonzalez, P., Grewe, K., Bao, G., Beuermann, S., et al. (2021). Extracellular matrix remodeling through endocytosis and resurfacing of Tenascin-R. 2021. Nat. Commun. *12*, 7129. https://doi.org/10.1038/s41467-021-27462-7.

58. Xiong, Y., Soumillon, M., Wu, J., Hansen, J., Hu, B., van Hasselt, J.G.C., Jayaraman, G., Lim, R., Bouhaddou, M., Ornelas, L., et al. (2017). A Comparison of mRNA Sequencing with Random Primed and 3′-Directed Libraries. 2017. Sci. Rep. *7*, 14626. https://doi.org/10.1038/s41598-017-14892-x.

59. Anders, S., Pyl, P.T., and Huber, W. (2015). HTSeq—a Python framework to work with high-throughput sequencing data. Bioinformatics *31*, 166–169. https://doi.org/10.1093/bioinformatics/btu638.

60. Dobin, A., Davis, C.A., Schlesinger, F., Drenkow, J., Zaleski, C., Jha, S., Batut, P., Chaisson, M., and Gingeras, T.R. (2013). STAR: ultrafast universal RNA-seq aligner. Bioinformatics *29*, 15–21. https://doi.org/10.1093/bioinformatics/bts635.

61. Schiebinger, G., Shu, J., Tabaka, M., Cleary, B., Subramanian, V., Solomon, A., Gould, J., Liu, S., Lin, S., Berube, P., et al. (2019). Optimal-Transport Analysis of Single-Cell Gene Expression Identifies Developmental Trajectories in Reprogramming. Cell *176*, 1517. e22. https://doi.org/10.1016/j.cell.2019.02.026.

62. Yu, G., Wang, L.-G., Han, Y., and He, Q.-Y. (2012). clusterProfiler: An R Package for Comparing Biological Themes Among Gene Clusters. OMICS.

63. Yu, G., and He, Q.-Y. (2016). ReactomePA: an R/Bioconductor package for reactome pathway analysis and visualization. Mol. Biosyst. *12*, 477–479. https://doi.org/10.1039/c5mb00663e.

64. Geiger, T., Wisniewski, J.R., Cox, J., Zanivan, S., Kruger, M., Ishihama, Y., and Mann, M. (2011). Use of stable isotope labeling by amino acids in cell culture as a spike-in standard in quantitative proteomics. Nat. Protoc. *6*, 147–157. https://doi.org/10.1038/nprot.2010.192.

65. Plubell, D.L., Wilmarth, P.A., Zhao, Y., Fenton, A.M., Minnier, J., Reddy, A.P., Klimek, J., Yang, X., David, L.L., and Pamir, N. (2017). Extended multiplexing of tandem mass tags (TMT) labeling reveals age and high fat diet specific proteome changes in mouse epididymal adipose tissue. Mol. Cell. Proteomics *16*, 873–890. https://doi.org/10.1074/mcp.m116.065524.

STAR★METHODS

KEY RESOURCES TABLE

REAGENT or RESOURCE	SOURCE	IDENTIFIER
Antibodies		
Mouse monoclonal anti OCT-3/4	Santa Cruz Biotechnology	Cat# sc-5279; RRID: AB_628051
Mouse monoclonal anti SSEA-4	Santa Cruz Biotechnology	Cat# sc-21704; RRID: AB_628289
Rabbit polyclonal Anti-KLF17	Atlas Antibodies	Cat# HPA024629; RRID: AB_1668927
Rabbit polyclonal Anti-TFE3	Atlas Antibodies	Cat# HPA023881
Mouse monoclonal anti-SUSD2	BioLegend	Cat# 327401
Mouse monoclonal anti-SUSD2-PE	BioLegend	Cat# 327406
Goat polyclonal anti-GATA-3	R&D Systems	Cat# AF2605
Goat polyclonal anti-SOX1	R&D Systems	Cat# AF3369
Goat polyclonal anti-SOX17	R&D Systems	Cat# AF1924
Goat polyclonal anti-Brachyury	R&D Systems	Cat# AF2085
Goat polyclonal anti-OTX2	R&D Systems	Cat# AF1979
Rabbit monoclonal anti-NANOG	Cell Signaling Technology	Cat# 4903S
Rabbit monoclonal anti-FOXA2	Cell Signaling Technology	Cat# D56D6; RRID: AB_10891055
Rabbit polyclonal Anti-SOX2	Novus Biologicals	Cat# NB110- 37,235; RRID: AB_792070
Rabbit polyclonal Anti-FOXG1	Abcam	Cat# Ab18259; RRID: AB_732415
Rabbit polyclonal Anti-COLLAGEN Type I	Abcam	Cat# Ab34710; RRID: AB_731684
Rabbit polyclonal Anti-COLLAGEN Type IV	Abcam	Cat# Ab6586; RRID: AB_305584
Rabbit polyclonal Anti-COLLAGEN Type VI	Fitzgerald	Cat# 70R-CR009x; RRID: AB_1283876
Rat monoclonal anti-INTEGRIN β1	Sigma-Aldrich	Cat# MABT821; RRID: AB_2891299
Rabbit polyclonal Anti-LAMININS	Sigma-Aldrich	Cat# L9393; RRID: AB_477163
Rabbit polyclonal Anti-VIMENTIN	Sigma-Aldrich	Cat# SAB1305445
Donkey anti-Rabbit IgG (H + L) Highly Cross-Adsorbed Secondary Antibody Alexa Fluor 488	ThermoFisher Scientific	Cat# A-21206; RRID: AB_2535792
Donkey anti-Rabbit IgG (H + L) Highly Cross-Adsorbed Secondary Antibody Alexa Fluor 647	ThermoFisher Scientific	Cat# A-31573; RRID: AB_2536183
Donkey anti-Mouse IgG (H + L) Highly Cross-Adsorbed Secondary Antibody Alexa Fluor 594	ThermoFisher Scientific	Cat# A-21203; RRID: AB_141633
Donkey anti-Goat IgG (H + L) Cross-Adsorbed Secondary Antibody Alexa Fluor 488	ThermoFisher Scientific	Cat# A-11055; RRID: AB_2534102
Donkey anti-Goat IgG (H + L) Cross-Adsorbed Secondary Antibody Alexa Fluor 647	ThermoFisher Scientific	Cat# A-21447; RRID: AB_2535864
Chemicals, peptides, and recombinant proteins		
Non-RGD-based antagonist ATN-161	Sigma-Aldrich	Cat# SML2079
Human FGF basic (154 aa)	Peprotech	Cat# 100-18B
Vitronectin (VTN-N) Recombinant Human Protein, Truncated	ThermoFisher Scientific	Cat# A14700
Matrigel	Corning	Cat# 354234
Matrigel growth factor reduced	Corning	Cat# 354230
MS-SAFE Protease and Phosphatase Inhibitor	Sigma-Aldrich	Cat# MSSAFE-1VL
SDS solution (10% in H20)	Sigma-Aldrich	Cat# 71736-100ML

(*Continued on next page*)

Continued

REAGENT or RESOURCE	SOURCE	IDENTIFIER
1M Triethylammonium bicarbonate (TEAB) for TMT experiments	ThermoFisher Scientific	Cat# 90114
DL-Dithiothreitol solution	Sigma-Aldrich	Cat# 43816-10ML
Sequencing grade modified trypsin	Promega	Cat# V5111
Pierce™ Trifluoroacetic Acid (TFA), Sequencing grade	ThermoFisher Scientific	Cat# 28904
Critical commercial assays		
RNeasy Plus Micro Kit	QIAGEN	Cat# 74034
RNeasy mini kit	QIAGEN	Cat# 74104
RNase-Free DNase Set	QIAGEN	Cat# 79254
SuperScriptTM VILO™ cDNA Synthesis kit	ThermoFisher Scientific	Cat# 11754250
Total RNA Purification kit	Norgen Biotek Corp.	N/A
M-MLV Reverse Transcriptase	ThermoFisher Scientific	Cat# 28025013
SYBR Green Master mix	Bioline	Cat# BIO-94020
Pierce™ BCA Protein Assay Kit	ThermoFisher Scientific	Cat# 23227
HiPPR Detergent Removal Kit	ThermoFisher Scientific	Cat# 88305
TMTsixplex™ Isobaric Label Reagent Set	ThermoFisher Scientific	Cat# 90061
TMT10plex™ Isobaric Label Reagent Set	ThermoFisher Scientific	Cat# 90110
Deposited data		
Proteomic data	This paper	MassIVE: MSV000086068, MSV000086069
RNA-seq data	This paper	GEO: GSE161717, GSE161371, GSE196050, GSE196157, GSE213024
Experimental models: Cell lines		
Human naive iPSCs HPD06 and HPD03	Giulitti et al., 2018[44]	N/A
Human primed iPSCs HPD00	Giulitti et al., 2018[44]	N/A
Human primed iPSCs Clone 7	Luni et al., 2016[28]	N/A
Human primed iPSCs HPD06	This paper	N/A
Human fibroblasts HFF-1	ATCC	Cat# SCRC-1041™
Mouse embryonic fibroblasts MEF DR4	ATCC	Cat# SCRC-1045™
Oligonucleotides		
Primers for qRT-PCR, see Table S5	ThermoFisher Scientific and Laboratory of Graziano Martello	N/A
Software and algorithms		
ImageJ (open-source GNU GPL v.3 license)	N/A	N/A
GraphPad prism 6	Dotmatics	N/A
MaxQuant v. 1.6.10.43	Wiśniewski et al., 2009[54]	N/A
MATLAB R2017a	The MathWorks	N/A
MATLAB R2019b	The MathWorks	N/A

RESOURCE AVAILABILITY

Lead contact

Further information and requests for resources and reagents should be directed to and will be fulfilled by the lead contact, Nicola Elvassore (n.elvassore@ucl.ac.uk).

Materials availability

The reagents described in this manuscript are available; requests for materials should be addressed to the lead contact.

Data and code availability

The authors declare that all data supporting the findings of this study are available within the article, its supplementary information, attached files, and online deposited data or from the authors upon reasonable request.

- Proteomic data have been deposited at MassIVE and are publicy available as of the date of publication. Bulk RNA-seq data have been deposited at GEO and are publicly available as of the date of publication. Accession numbers are listed in the key resources table and below. Microscopy data reported in this paper will be shared by the lead contact upon request. MassIVE: MSV000086068, MSV000086069. GEO: GSE161717, GSE161371, GSE196050, GSE196157, GSE213024.
- This paper does not report original code.
- Any additional information required to reanalyze the data reported in this paper is available from the lead contact upon request.

EXPERIMENTAL MODEL AND SUBJECT DETAILS

Cell lines

Human naive induced pluripotent stem cells (naive hiPSCs, HPD06 and HPD03),[44] primed induced pluripotent stem cells (hiPSCs; Clone7,[28] HPD06 and HPD00[44] lines), fibroblasts (HFF-1, ATCC) and mouse embryonic fibroblasts (MEF, DR4, ATCC) were employed for this study. The transcriptomic, metabolic and epigenetic profiles of naive lines were extensively characterized in Giulitti et al. to confirm their similarity to other naive cell lines. The human primed HPD06 line was specifically generated for this study as detailed below. Key findings were confirmed in both HPD06 naive vs induced primed (isogenic, HFF-derived), and in HPD03 naive vs HPD00 primed (isogenic, BJ-derived).

Cell culture in 2D

Pluripotent cell lines were cultured at 37°C, 5% CO_2 and 5% O2 atmosphere, fibroblast at 37°C and 5% CO_2 atmosphere. Cell lines were routinely tested and confirmed negative for mycoplasma.

Naive hiPSCs were cultured on a confluent layer of mitotically inactive MEFs (DR4, ATCC) in RSeT™ medium (Stemcell Technologies). Cells were passaged every 4-5 days with TrypLE Select Enzyme (Life Technologies) as previously described.[44] Primed hiPSCs were expanded in wells (Corning) coated with 0.5% Matrigel growth factor reduced (MRF, Corning), cultured in Essential 8 medium (E8, Stemcell Technologies) and passaged every 4-5 days with EDTA (ThermoFisher Scientific). Medium change was performed every 24h for both naive and primed hiPSCs. HFF cells were cultured on 100 mm Petri dishes (Falcon) in High Glucose Dulbecco's modified Eagle Medium (DMEM, ThermoFisher Scientific) supplemented with 10% Fetal Bovine Serum (FBS, ThermoFisher Scientific). Medium was changed every second day.

Cell short-term cultures in microfluidic devices

Microfluidic chips were produced as previously described.[44] Each microfluidic chip was placed in a 100 mm Petri dish with 1% Penicillin/Streptomycin in phosphate buffer without Ca2+/Mg2+ (PBS) (ThermoFisher Scientific) to maintain sterility and controlled humidity. Each channel was washed once with PBS to remove any possible debris and coated with 0.5% MRF (Corning) or 50/100 μg/mL vitronectin (VTN, ThermoFisher Scientific) for 1 h at room temperature. Naive hiPSCs optimal seeding density was defined as 400 cells/mm^2. A standard seeding volume of 12 μL was necessary to ensure a homogeneous cell seeding through the inlet and along the culture chamber. Medium change was performed every 12 h.

Cell expansion in 3D

Naive cells were switched from 2D to 3D culture by detaching naive colonies from 2D MEF, dissociating the colonies as single cells with TrypLE and then embedding them in 100% Matrigel (Corning) drops as described below. Optimal cell density was defined as 2k cells/μl, and 25μL of this was spread on tissue culture treated multiwell plates (Falcon) for maintenance. Medium change was performed every 24 h and cells were passaged every 4 - 5 days. After 2 passages in 3D, we confirmed the absence of MEF contamination.

To passage 3D cultured cells, we developed the following protocol: Matrigel drops were washed once with cold PBS without calcium or magnesium to destabilize the gel. Then, TrypLE was added, and drops were mechanically broken by pipetting 3-4 times, followed by incubation for a total of 12 min at 37°C. At minute 8, more pipetting helped to break leftover Matrigel clumps. TrypLE was inactivated by adding cold 20% KSR in DMEM/F12. A single cell solution was obtained by pipetting and cells were collected in cold falcon tubes. Cells were counted and centrifuged at 1800 rpm, for 5 min at +4°C. Supernatant was discarded and cells were resuspended with Matrigel at the density of 2k cells/μl. Seeding volumes were chosen according to experimental necessity, for high volume drops it was essential to spread slightly the Matrigel to increase volume/surface ratio thus avoiding cells in the center of the drop to suffer from nutrient shortage. Plates with drops were kept at 37°C for 5–10 min (according to drop dimension) to let the Matrigel jellify, then warm (37°C) RSeT supplemented with 10 μM StemMACS Y27632 ROCK Inhibitor (Ri, Miltenyi Biotech) was added to the cells. For smaller drops, adding PBS in the closest wells during jellification was beneficial to control humidity thus preventing drops from drying.

METHOD DETAILS

ECM treatments and clonogenicity assay

Naive hiPSCs were seeded in microfluidic devices, on feeders, at the density of 400 cells/mm^2, in RSeT media and in hypoxic conditions. One day after seeding, the following media were used: RSeT medium (control); RSeT medium supplemented with *i*) 100 μg/μL

non-RGD-based antagonist ATN-161 (Sigma, SML2079); *ii*) 50 μg/mL blocking antibody anti-integrin β1 (Sigma, MABT821), *iii*) 2 μg/mL antibody anti-laminins (Sigma, L9393); *iv*) 1 μg/mL antibody anti-collagen IV (Abcam, ab6586); *v*) 4 μg/mL antibody anti-collagen VI (Fitzgerald, 70R-CR009x); *vi*) an antibody that doesn't target ECM components (mock Ab, 2 μg/mL antibody anti-FOXG1, Abcam, ab18259). For anti-ECM antibody treatments, we extended already reported protocols that target ECM components by administering antibodies in living systems.[55–57] Used antibodies are listed in Table S4. Media was changed every 12 h, and cells were cultured for 5 days in total. Samples were monitored during culture with brightfield imaging, fixed after 5 days and SUSD2 immunostained for mean fluorescence intensity quantification (details are reported in the section "imaging analysis and quantification").

Clonogenicity assay was performed for untreated samples and cells treated with anti-laminins or anti-collagen VI or anti-mock antibodies, cultured as described above. Naive hiPSCs were collected as single cells from the microfluidic devices, counted, resuspended in RSeT and seeded at clonal density (95 cells/well) in 384 well plates (PerkinElmer). Cells were cultured in RSeT supplemented with 10 μM StemMACS Y27632 ROCK Inhibitor (Ri, Miltenyi Biotech) for the first 2 days, and then cultured in RSeT for other 3 days. To quantify naive hiPSCs clonogenicity, cells were fixed (5 days of culture), immunostained for NANOG and KLF17, and imaged to quantify double-positive NANOG + KLF17 + colonies.

Naive to primed conversion in 2D

HPD06 Naive cells were converted into an isogenic primed line with the following protocol. Cells have been cultured in 12-well multiwell (Falcon) on MEF in RSeT medium. The day before passaging, considered as the first day of transition, medium was changed to N2B27 medium (DMEM/F12-Neurobasal medium 1:1, ThermoFisher Scientific, 1% B-27 Supplement, ThermoFisher Scientific, 0.5% N-2 Supplement, ThermoFisher Scientific, 1% GlutaMAX Supplement, Life Technologies, 1% MEM Non-Essential Amino Acids Solution 100x, Life Technologies, 0.01% 2-Mercaptoethanol, Life Technologies, and 0.25% Insulin 1.72 mM, Sigma-Aldrich). Then cells were dissociated at single-cell with TrypLE for 5 min at room temperature, inactivated with equal volume of 0.5 mg/mL Soybean Trypsin Inhibitor (ThermoFisher Scientific) and centrifuged at 300 g for 5 min. Cells were seeded on 0.5% MRF coating in N2B27 medium supplemented with 10 μM Ri. From the day after, medium was gradually switched from N2B27 to E8, following this gradient: day 3 75% N2B27 + 25% E8; day 4 50% N2B27 + 50% E8; day 5 25% N2B27 + 75% E8 and day 6 100% E8. When colonies with primed-like, flat morphology appeared cells were passaged with 0.5 mM EDTA on 6-well multiwell (Falcon) coated with 0.5% MRF, in E8 medium, and passaged until stable.

Naive to primed conversion in 3D

To induce naive iPSCs toward a primed identity in 3D Matrigel, we developed the following protocol. Naive cells previously cultured in 3D Matrigel were dissociated to single-cell with TrypLE following the passaging procedure described above, and seeded at the same 2k/μl density as for 3D cell maintenance. Once jellified, Matrigel-embedded cells were instead fed with E6 (Gibco) + FGF2 (20 ng/mL, PeproTech) supplemented with Ri. After 24h Ri was withdrawn and, 5 days after seeding, E6 + FGF2 medium was replaced with E8.

Extra-embryonic multilineage differentiation in 2D

Naive cells coming from 3D culture systems were induced toward Primitive endoderm differentiation following the protocol previously described.[42] Conversion of human naive PSCs into trophoblast stem cells (TSCs) was obtained by pre-treating cells, cultured on MEFs, with trophoblast stem cell (TS)[45] medium for 24 h. Then naive hiPSCs were single-cell dissociated and replated on 12-well plates, pre-coated with 5 μg/mL of Collagen IV (Corning), at the density of 0.25-0.5 x 10^6 cells/well and cultured in TS medium. hTSCs were then cultured as previously described in Okae et al.

Multilineage differentiation in 2D

Naive cells coming from 3D culture systems were induced toward germ layer differentiation as previously described.[44] Cells obtained after the 3D priming were induced toward definitive mesoderm,[51] definitive endoderm[52] and neuroectoderm[50] germ layer differentiation as previously described.

Blastoid generation

Naive cells coming from 3D culture systems were passaged as single cells and seeded in low adhesion U-bottom culture plates to induce blastoid formation following the protocol previously published.[48]

Electron microscopy imaging

Naive and primed lines were cultured both on glass coverslips and microfluidic devices and fixed 4 days after seeding for the analysis. Naive cells were cultured on MEF feeder layer while primed cells were cultured on 2.5% MRF. Cells undergoing SEM observation were first washed with PBS, then fixed with Glutaraldehyde 2.5% in Cacodylate buffer 0.1 M pH 7.4 (both Sigma-Aldrich), rinsed with Cacodylate buffer 0.1 M pH 7.4, post-fixed with OsO4 1% in Cacodylate buffer 0.1 M pH 7.4, dehydrated in an ethanol series, dried by critical point drying (Balzers CPD 030, Balzers A.G., CH), mounted on aluminum stubs, sputtered with gold in an Edwards S150B apparatus (Edwards Vacuum Italy) and observed with a Zeiss EVO MA10 SEM (Carl Zeiss Oberkochen, Germany) at 20 kV. For TEM imaging cells were washed once with PBS, fixed with Glutaraldehyde 2.5% in cacodylate buffer 0.1 M pH 7.4 and 1% osmium tetroxide in cacodylate buffer 0.1M, and embedded in Epon812. Ultrathin sections were stained with lead citrate and uranyl acetate and observed with a Philips EM400 electron microscope operating at 100 kV.

Immunohistochemistry

Naive, primed, MEF only and HFF cells were cultured on glass coverslips and in microfluidic chips and fixed 4 days after seeding for immunofluorescence characterization. Naive cells were seeded on MEF and primed cells on 2.5% MRF. MEF and HFF were cultured on 25 μg/mL VTN. Cells were fixed with 4% paraformaldehyde (Sigma-Aldrich) in $PBS^{-/-}$, 10 min at room temperature. Permeabilization and blocking were performed simultaneously by incubating samples with 10% FBS in $PBS^{-/-}$ with 0.1% (v/v) Triton X-100 (Sigma-Aldrich) for 1 h at room temperature. Then cells were incubated over-night at +4°C with primary antibodies, diluted in blocking solution. The day after, samples were washed with PBS −/− three times for 5 min and then incubated with secondary antibodies, diluted in blocking solution. Incubation was performed for 45 min at 37°C. Samples were washed again with PBS, three times for 5 min, and then mounted with 80% glycerol (Sigma-Aldrich) in PBS −/−.

3D cultured cells and blastoids were fixed with 2% paraformaldehyde in $PBS^{-/-}$, 45 min at room temperature. Permeabilization and blocking were performed simultaneously by incubating samples with 1% BSA (Sigma Aldrich) in $PBS^{-/-}$ with 0.5% (v/v) Triton X-100 for 3 h at room temperature. Then samples were incubated 24 h at +4°C with primary antibodies, diluted in blocking solution. The day after, samples were washed with blocking solution three times for 15 min and then incubated 24 h at +4°C with secondary antibodies, diluted in blocking solution. Samples were then washed once with blocking solution for 15 min, then with PBS −/− two times for 15 min. Samples were adapted to and then mounted in Fluoromount-G (Southern Biotech). Blastoids were imaged in PBS −/− in multiwell plates with glass bottom. All primary and secondary antibodies used are listed in Table S4. Nuclei were stained with Hoechst 33,342 (Thermo Scientific) and F-Actin with Phalloidin 488 or 647 (Invitrogen). Confocal fluorescence images were acquired using a TCS SP5 microscope (Leica Microsystems). 2D monolayer differentiation widefield fluorescence images were acquired using a DM IL LED microscope (Leica Microsystems).

Imaging analysis and quantification

We used ImageJ software for adjustments of levels and contrast, maximum and SD intensity projections, 3D reconstructions and thresholding to create binary masks used for quantification of SUSD2 immunostained samples. To quantify the mean fluorescence intensity of SUSD2 at least 3 imaged channels per microfluidic device of independent biological triplicates for each sample were converted in binary masks and used for analysis with ImageJ software (open-source GNU GPL v.3 license). For clonogenicity assay, double-positive NANOG + KLF17 + colonies were manually counted from 6 independent biological replicates.

RNA sequencing and transcriptomic analysis

We performed bulk-RNA sequencing of samples extracted from HFF fibroblasts, HPD06 primed and HPD06 naive cells, all cultured in normoxic conditions both on glass coverslips and in microfluidic devices. Samples were collected at day 1, 4 and 7 after seeding. Fibroblasts were seeded on 25 μg/mL VTN, primed iPSCs on 2.5% MRF and naive iPSCs on MEFs. RNA was extracted with RNeasy Plus Micro Kit (Qiagen) following manufacturer instructions.

We also performed bulk-RNA sequencing of samples collected from microfluidic culture of HPD06 naive cells on MEFs, naive seeded on 50 μg/mL VTN and MEF feeders alone seeded on 50 μg/mL VTN, all in RSeT media in hypoxic conditions. RNA was collected with RLT lysis buffer. RNA extraction from microfluidic channels was performed in triplicates from each condition, each replicate made by pooling together the lysates obtained from 3 channels.

We performed bulk-RNA sequencing of HPD03 naive hiPSCs collected from 3D feeder-free culture or 2D culture on feeders. Cells were cultured in both conditions in parallel, always at the same passage number, and were harvested as described in the cell expansion in 3D section. Prior to lysis, cells were live-stained with anti-SUSD2 antibody (Table S4) and sorted by fluorescence-activated cell sorting (FACS). Briefly, cells were centrifuged and resuspended with $PBS^{-/-}$ supplemented with 10 μM StemMACS Y27632 ROCK Inhibitor and with/without the SUSD2 antibody (used according to manufacturer's recommendation). Cells were stained for 10 min at room temperature in the dark, then washed and resuspended with 20% KSR in DMEM/F12 supplemented with 10 μM StemMACS Y27632 ROCK Inhibitor to sustain cell viability. FACS was performed with the BD FACSAria™ IIIu (BD biosciences), excluding dead cells by adding DAPI (ThermoFisher Scientific) at 0.05 ug/ml. Samples were collected sorting for DAPI negative cells (Bulk) and DAPI negative and SUSD2 positive (SUSD2+) cells. Samples were collected in quadruplicates for each culture condition and each sorted population, at passage 6 and passage 10 of culture, lysed with RLT buffer and then RNA was extracted using RNeasy Plus Micro Kit (Qiagen).

We also performed bulk-RNA sequencing of 3D naive hiPSCs, naive priming in 3D Matrigel at 2, 4, 6, 8 and 10 days of differentiation, and isogenic primed hiPSCs cultured in 3D for 4 days in their standard E8 maintenance media. 3D priming was performed as described in the related section. Four replicates were collected for each sample type. To collect the RNA samples, naive colonies, primed and priming cysts were extracted from the Matrigel drops then lysed with RLT buffer. RNA was extracted using RNeasy Plus Micro Kit (Qiagen).

Total RNA was quantified using the Qubit 2.0 fluorometric Assay (Thermo Fisher Scientific). Libraries were prepared from 100 ng of total RNA using the NEGEDIA Digital mRNA-seq research grade sequencing service (Next Generation Diagnostic srl)[58] (which included library preparation, quality assessment and sequencing on a NovaSeq 6000 sequencing system using a single-end, 100 cycle strategy (Illumina Inc.). Illumina NovaSeq base call (BCL) files were converted into fastq files through bcl2fastq (2019) (version v2.20.0.422). The raw data were analyzed by NEGEDIA Digital mRNA-seq pipeline (v1.0) which involves a cleaning step by quality filtering and trimming, alignment to the reference genome and counting by gene (BBMap – Bushnell B. – sourceforge.net/projects/bbmap/;[59,60]). The raw counts obtained were subsequently expressed as counts per million (CPM). After that the genes that

did not have at least 2 CPM in one or more samples were filtered out. For the hypoxia samples, the alignment was performed using a hybrid hg38/mm10 genome obtained by combining the two single genomes (NCBI Annotation release 93). The expression levels of genes were expressed as CPM. Only human genes that had 2 or more CPM in at least one of the samples were considered. Differentially expressed genes (DE-Gs) were computed with edgeR starting from raw count data (Robinson et al., 2009), using a mixed criterion based on p value, after false discovery rate (FDR) correction by Benjamini Hochberg method, lower than 0.05 and absolute log2(fold change) higher than 2.

PCA was performed by Singular Value Decomposition (SVD) on log2(CPM+1) data, after centering, using MATLAB R2017a (The MathWorks). Naive gene selection was taken from previously published works.[19,20] MEF identity genes were randomly selected from those reported in Schiebinger et al. (2019),[61] we also manually added Thy1 and Cdh2 as well-recognized typical fibroblast markers. Enrichment analyses within Gene Ontology-Biological Process (GO-BP) and Reactome databases were performed in R (v. 4.0.3) using clusterProfiler[62] (v. 3.18.0) and ReactomePA[63] (v. 1.34.0) Bioconductor packages, respectively, with FDR-corrected p value lower than 0.01. Hierarchical clustering with heatmap data visualization was performed using Euclidean distance and complete linkage. ECM genes were classified according to the annotations in Hynes and colleagues (2012).[31]

For RNA-seq from HPD03 naive hiPSCs collected from 3D feeder-free culture or 2D culture on feeders, alignment, quantification, normalization, and gene selection was performed as in Figure 3C in Giulitti et al. (2018), to allow direct comparison with published RNA-seq data in the same Principal Component Analysis (PCA). List of all the cell lines showed in the resultant PCA (Figure 5F) can be found in Table S6.

For RNA-seq from 3D priming samples, total RNA was quantified using the Qubit 2.0 fluorometric Assay (Thermo Fisher Scientific). Libraries were prepared from 600 to 1000 pg of total RNA using the SMART-Seq v4 Ultra Low Input Kit (Takara Bio) followed by Nextera XT DNA Library Preparation kit (Illumina). Libraries were sequenced on a NovaSeq 6000 sequencing system using a paired-end, 100 cycle strategy (Illumina Inc.). Illumina NovaSeq 6000 base call (BCL) files were converted in fastq file through bcl2fastq. Alignment was performed with STAR 2.6.0a[59] using hg38 reference genome and the expression levels of genes were determined with RSEM 1.3.0.

Genes were annotated with the Ensemble database and raw counts were expressed as counts per million (CPM). Data was filtered to keep only genes with more than 10/min (library size*10∧-6) count per million (CPM) in more than three replicates in at least one sample and normalized by negative binomial distribution (TMM) with EdgeR. PCA was performed on log2(CPM+1) data using R (v. 4.1.3). Differentially expressed genes (DE-Gs) analysis was performed using edgeR on processed data, using a p value, after FDR correction by Benjamini Hochberg method, lower than 0.01 and absolute log2 (fold change) higher than 2 as thresholds. This analysis was applied on every paired combination of samples from the timecourse. The union of all found DE-Gs was used for further analyses. DE-Gs were assigned to five clusters, as in Rostovskaya et al., (2019), using *k*-means algorithm implemented in MATLAB R2019b (The MathWorks) and the genes temporal profiles for each of the clusters were represented. A comparison between the DE-Gs found for each paired combination of samples was performed graphically with Venn diagrams using R Eulerr (v. 6.1.1) package. Heatmap data visualization was performed using lists of selected genes compiled from KEGG pathways and published literature.[44,49,53]

Quantitative reverse transcriptase PCR

Total RNA was extracted using RNeasy mini kit, according to manufacturer's spin protocol (QIAGEN) including the RNase-free DNase (QIAGEN) step to digest contaminant DNA. cDNA was produced from $\leq$300 ng RNA using SuperScript™ VILO™ cDNA Synthesis kit, following the recommended protocol (Invitrogen). qRT-PCR reactions were performed using the Taqman Gene Expression Master Mix (Thermo Fisher Scientific). Gene expression relative to *GAPDH* in each well was determined using VIC-labelled *GAPDH* probe together with FAM-labelled TaqMan assay probe (Applied Biosystems) which are listed in Table S5.

For trophoblast stem cell (TSC) differentiation analysis, total RNA was isolated using a Total RNA Purification kit (Norgen Biotek), and cDNA was made from 500 ng using M-MLV Reverse Transcriptase (Invitrogen) and dN6 primers. For real-time PCR, SYBR Green Master mix (Bioline, BIO-94020) was used. Primers are detailed in Table S5. Three technical replicates were performed for all qRT-PCR experiments. *GAPDH* was used as the endogenous control to normalize expression.

Conditioned medium, total lysates and decellularization for proteomic analysis

Naive hiPSCs were purified from MEF contaminants by multiple passages on ECM coated plates. Cells were then dissociated as single cells and seeded in microfluidic devices at the density of 400 cells/mm^2 on MEFs, and on 50 μg/mL VTN. In parallel, MEF feeders alone were seeded on 50 μg/mL VTN in RSeT medium. Conditioned media were collected every 12h for 3 days, in triplicates for each condition. Each replicate was constituted by the media from 10 microfluidic channels pulled together. To each replicate MS-SAFE Protease and Phosphatase Inhibitor was added according to manufacturer's instruction (Sigma Aldrich). Total lysates were collected at day 3 from each condition, three replicates were made from the lysates of 10 channels pooled together. Lysates were collected by washing first the channels with PBS$^{-/-}$ then by removing the PBS, cutting the roof of each microfluidic channel and scratching with 20 μL of 4% SDS in Ultrapure distilled water (ThermoFisher scientific). To the lysis buffer MS-SAFE Protease and Phosphatase Inhibitor was added according to manufacturer's instruction. All samples for the proteomic analysis were stored at −80°C prior to the analysis.

Proteomic sample pre-processing

Before BCA protein quantification (Thermo Fisher Scientific), centrifuge-aided filtration in Amicon-Ultra 10 kDa cut-off spin-column (Millipore) was performed for buffer-exchange to 8 M urea (Sigma-Aldrich) in 50 mM TEAB buffer (Thermo Fisher Scientific). Centrifugation was performed at room temperature for 10 min at 14,000g with freshly prepare urea buffer with 4 rounds of 1:5 dilution of the protein concentrate.

Standard samples were prepared for normalization purposes and quality control of technical variability.[64] The first batch of standard samples was composed by an equal amount of all lysate samples and added in duplicate into the TMT6 sample described below. The second batch of standard samples was composed of an equal amount of all conditioned media samples and added in duplicate into the TMT10 samples described below. All samples for total lysates (30 μg of input protein per condition), conditioned media (40 μg of input protein per condition) and relative standards were subsequently processed identically.[54] Briefly, protein reduction with 5 mM DTT (Sigma-Aldrich) was carried out in 50 μL of 50 mM TEAB for 60 min at 37°C with 800 rpm shaking, followed by alkylation with 20 mM iodoacetamide (Sigma-Aldrich) for 30 min at 25°C protected from light. After diluting the samples 1:10 with 50 mM TEAB, tryptic digestion was carried out with 2 μg of trypsin (Promega) per reaction for 20 h at 37°C with 800 rpm shaking and supplemented with TFA to a final 0.2% concentration to stop the reaction. Samples were desalted with MonoSpin C-18 columns (GL Sciences) and speed-vacuum evaporated over-night. After reconstituting the peptides in 100 μL of 50 mM TEAB, TMT-conjugation was performed according to the supplier's instructions (one TMT 6-plex for "total lysate" samples, and three TMT 10-plex for "conditioned media" samples, both from Thermo Fisher Scientific), speed-vacuum evaporated over-night, desalted and speed-vacuum evaporated once again. In order further reduce detergent contamination, all samples were reconstituted in 100 mM ammonium bicarbonate (Sigma-Aldrich) and processed with HiPPR Detergent Removal Kit (Thermo Fisher Scientific) twice, before liquid chromatography fractionation (16 fractions per sample) and mass spectrometry analyses.

Protein identification by liquid chromatography–tandem mass spectrometry (LC-MS/MS) was performed using Thermo Fusion Mass Spectrometer with Thermo Easy-nLC1000 Liquid Chromatography. 130 min of LC-MS gradients were performed by increasing organic proportion. The first level of MS was detected by Orbitrap with parameter of Resolution at 120 K, Scan Range at 300–1800 *m/z*, Mass Tolerance at 10 ppm. The second level of MS was isolated by Quadrupole, activated by HCD and detected by Orbitrap. The Orbitrap Resolution for the second level of MS was 30 K.

Proteomic bioinformatics analysis

Peak list files were searched against UniProt human reference proteome (UP000005640) by MaxQuant v. 1.6.10.43[64]. TMT6 or TMT10 modifications and carbamidomethyl on cysteine were set as fixed modifications. The oxidation of methionine and acetylation of protein N-terminus were set as variable modifications. Peptide-spectrum matches (PSMs) were adjusted to 1% and then assembled further to a final protein-level false discovery rate (FDR) of 1%. Reverse proteins and contaminants, proteins not quantified in any sample, proteins identified without unique peptides in any sample or with a q-value > 0.01 were filtered out. TMT6 intensities, i.e. lysate samples, were normalized within the same TMT sample by scaling the median of each sub-sample (Figures S3A–S3D). TMT10 intensities, i.e. media samples, were normalized only between different TMT samples according to Plubell and colleagues[65] (Figures S3A–S3D).

Bioinformatic analysis was performed in MATLAB R2017a (The MathWorks) using normalized log2 (TMT intensities). Hierarchical clustering with heatmap data visualization was performed using Euclidean distance and complete linkage. ECM genes were classified according to the annotations in Hynes and colleagues.[31] Functional enrichment analysis of Reactome pathways and GO-BP categories was performed using ReactomePA[63] and ClusterProfiler[62] Bioconductor packages, respectively. Differentially accumulated proteins in conditioned media were identified by ANOVA with FDR-corrected p value < 0.05, followed by Tukey's post-hoc test with p value < 0.05. Proteins identified as accumulated in MEF, Naive on VTN and Naive on MEF at day 2 or 3 respect to RSeT samples were classified as secreted by MEF, naive or both cell types, respectively.

QUANTIFICATION AND STATISTICAL ANALYSIS

All analyses were performed with GraphPad prism 6. We expressed data as mean ± SD of multiple biological replicates (as indicated in the figure legend). We determined statistical significance by unequal variance Student's *t* test, one-way ANOVA and Tukey's multiple comparison test. A p value of less than 0.05 was considered statistically significant.